Bachelor Graduation Thesis

Medical Sensor System

Johan van den Brink
Robbert Friendwijk

System designed for:
Non-invasive 'Sensor Patch' used to monitor newly born infants

TU Delft

Bachelor Graduation Thesis

Medical Sensor System

by

Johan van den Brink
Robbert Friendwijk

To obtain the degree of Bachelor of Science
at the Delft University of Technology,

Student number:	Johan van den Brink	4591925
	Robbert Friendwijk	4567331
Project duration:	March 30, 2020 – June 19, 2020	
Thesis committee:	Prof. dr. ir. G. de Graaf,	TU Delft, supervisor
	Prof. dr. ir. M.A.P. Pertijs,	TU Delft
	Dr. C. García Almudever,	TU Delft
	Prof. dr. J. Dudink,	UMC Utrecht

TU Delft

Abstract

In this research a sensor patch for newborns is proposed. This sensor patch is a device which would be attached to the skin of a newborn in order to monitor vital health signs such as: temperature, heart rate, respiration rate and oxygen saturation. Furthermore, a bilirubin sensor will be included to check the newborn for jaundice. Thereafter, the measured data should be communicated wirelessly to a base station. What happens with the data after the base station is beyond the scope of this research. One of the main challenges is energy efficiency since the patch should be small enough to fit on a newborn which means the battery should be small as well. Additionally the sensor patch should be able to operate for 3 days continuously.

The overall design is divided into three subsystems: the battery control system, the microcontroller and communication and the sensors. This report focuses on the sensor part of the total system.

After analysis of different kind of sensors, the SI7051 is chosen for the temperature sensor since it is the most accurate and energy efficient. In order to measure the respiration rate an acceleration sensor was chosen to be the most suitable within the system requirements. For the acceleration sensor the IIS2DLPC was selected. In order to measure the heart rate and oxygen saturation a PPG sensor is designed. Finally, the bilirubin sensor is designed which uses PPG as well.

However, the designed sensors still need calibration by empirical experiments in order to obtain accurate results.

Preface

This report was written in spring/summer of 2020. At this time, Covid-19 has caused limitations on the research. Due to the disease many facilities at the university were not available. During the report it will sometimes be mentioned that due to circumstances certain actions were not possible. This refers to the covid-19 situation.

This project is part of the bachelor graduation project of 6 students at Delft University of Technology. The group of students is split up in smaller groups of 2 students which each solve a part of the design. The research was proposed by dr. ir. G. de Graaf who works at the microelectronics department of the Delft University of Technology. After the proposal was accepted by the students, they came into contact with dr. Dudink who is a specialist in neonatology and neoroscience. With his help, a better understanding about what the design should look like was found.

Acknowledgments

During this project there have been several people who contributed to our design voluntarily. We are very grateful for that and would like to thank them. A special thanks to our supervisor Dr.ir. G. de Graaf for all his time and advice in the guiding of the project and writing of the report. Finally, a special thanks to Dr. J. Dudink for his advice on healthcare.

Contents

1 Introduction

1.1. Problem definition

Maternity care has always been a big concern in hospitals. It has also developed a lot over the course of the years. It was long thought that for instance babies were unable to feel pain[25]. Recently there has also been more attention for the psychological effects on newborns on neonatal intensive care[9]. It was discovered there is a relationship between the bonding of a newborn with its mother in the first couple of days and long-term emotional well-being of the newborn.

Due to the rising awareness of this fact, hospitals are trying to improve the amount of contact a parent can have with their child [8]. One particular solution includes using a sensor patch with NFC. This way it is possible to remove all wires from the body of the the newborn. This allows the parents to pick up the newborn, thereby making it easier to bond with the newborn. This is a clever solution using NFC, but it is mainly meant for hospitals.

In order to improve the bonding between parents and newborns even further, the baby should be able to go home as soon as possible. However, newborns that are in the risk category should still be monitored. Therefore a wireless sensor patch is needed that can fulfill all the tasks that would have been done by nurses at the maternal care in the hospital. This allows for better bonding with the parents, is cheaper than keeping newborns in the hospital and could trace diseases early in newborns to prevent disease.

Scoping and bounding

The objective in this report is to provide a theoretical design of the sensor patch. The sensor patch will be designed in such a way that it can measure, process, and deliver the data to a base station. The base station, in short, will be a device that receives the data wireless from the sensor patch. What happens after the data reaches the base station is beyond the scope of this research. For real implementation of this design, a sort of IT infrastructure would be needed to handle the data but this will not be covered in this report either.

Due to current circumstances the necessary experiments could not be performed. These experiments would be needed in order to:

- calibrate the sensors of the sensor patch
- provide the actual total power consumption of the designed system
- accurately analyse and compare the power consumption of different microcontrollers and communication modules

1.2. State of the art analysis

Wireless sensors are gaining territory in the a wide range of applications. This is due to their increasingly smaller sizes, lower power consumption and increase in energy harvesting efficiencies. A wide range of wireless sensor nodes are developed such as office sensors[2], machine health monitoring [5] and medical sensors

[33]. In addition, a lot of research has been done in biomedical wireless sensors field already. Wireless sensors measuring heart rate, temperature, oxygen saturation and many more are already common in patches or implants [20]. Also systems with real-time monitoring are being developed for for instance cough detection, breathing rate [7] and electrocardiogram (ECG) measurements [8].

The main concern in such products is battery life. The battery life is determined by the battery capacity and energy consumption. In consumption, the wireless communication often has the largest share. However, Battery life increased a lot recently. This is due to both increases in miniature battery capacity [30] and low-power reliable communication protocols [27].

Most designs are however not yet adapted to health care situations that give rise to very specific requirements. Most designs are made to measure vital functions and are made for adults, while much progress can also be made in more specific applications. An example of this is about research in wireless sensor node in neonatal intensive care in hospitals [8]. However, hardly any research has been done toward a design that can help monitor newborns at home.

1.3. Thesis synopsis

The thesis has the following structure. Chapter 2 will describe the requirements for the total system (the Sensor Patch) and the design requirements for the sensor system. Furthermore the decomposition of the total system is described here. Chapter 3 contains an elaborate study of the different methods for measuring medical parameters and results in the used measuring techniques for the sensor system. Chapter 4 lists multiple sensors utilizing the measuring methods chosen in chapter 3 and analyses their performance and specifications to determine the best sensor for the system. Chapter 5 contains the deign process for a photoplethysmography (PPG) sensor capable of measuring heart rate, oxygen saturation and bilirubin. The design is based on theoretical models as no prototype could be made and tested. Finally in chapter **??** final conclusions are drawn and recommendations are made for future work.

2

Program of requirements

2.1. Background

Every year, a lot of babies end up in maternity care. This is a very costly environment for the baby to be in. Next to this, the environment causes a lot of stress for the babies. In addition, there are some babies every year that are not monitored enough in home care. The consequence of wrong monitoring at home results in permanent handicaps due to jaundice for 10 babies each year in just the Netherlands. Therefore, the goal of this project is to replace the maternity care with a sensor patch.

In order to outperform maternity care in hospitals, the sensor patch should at least measure all the parameters the nurses measure. Next to that, it should also do this at least as frequently as the nurses do. In the Netherlands, a baby in maternity care often stays there for around 2-3 days. Nurses in maternity care check on babies every 4 hours and check the following parameters:

1. Temperature
2. Heart rate
3. Respiration rate
4. Oxygen saturation
5. General appearance of the skin, including an assessment of jaundice.

This last point, general view at skin, means the nurse checks whether the baby looks healthy overall. This is done to get an impression of whether the baby might have underlying conditions that are hard to monitor with current technology. Jaundice is one of the most important examples of these conditions.

In addition, measurements performed in hospital maternity care involve multiple wired electrodes to be attached to the babies. This decreases comfort for babies and can increase their stress levels. Secondly, for the parents of the newborns this is not a pleasant sight.

2.2. Requirements of entire system

Based on the previously sketched background and consultations with J. Dudink [1] the requirements of the entire system can be described in greater detail. J. Dudink is a specialist in neonatology and neoroscience. From 2004 to 2016 he has worked as a neonatologist and researcher of neonatal neuroimaging at Erasmus Medical Center. J. Dudink is presently working at the Department of Neonatology at University Medical Center Utrecht.

During the consultations with Dr. Dudink, it was decided that the sensor patch should be located on the baby's chest. At this location, the sensor patch is not prominently visible, which is pleasant for the parents.. Moreover, there is more room for the sensor patch here than in other places. In addition, the doctor stated that the size of the sensor patch may not exceed 70mm x 30mm x 10mm (L x W x H). In order to outperform

the maternity care, as it is now the sensor patch will need to perform measurements at least once every two hours to improve on the once every four hours in hospitals, in order to provide data significantly more frequent. In addition, at least the same measurements as maternity care must be carried out to guarantee at least the same level of care. This means that at least temperature, heart rate, oxygen saturation and bilirubin need to be measured. Furthermore the sensor patch needs to last for 3 days without the need to perform a recharge of the battery as this is how long babies are monitored in hospitals. In modern life, environmental awareness plays an important role. The sensor patch can eventually be used on many newborn babies, creating a lot of electronic waste if it is not reusable. It would be irresponsible not to take this into account during the design process. Moreover, one of the goals of the world health organization is to create less waste and environmental impact [21]. Therefore it was decided that the sensor patch has to be reusable and preferably usable for at least 1 year with 2 uses every week. This does mean that it must be possible to clean the sensor patch to medical standards and preferably to make it sterile.

The previous defined requirements are divided between mandatory requirements and trade-off requirements. Mandatory being the requirements which are absolutely essential for the system to be marked a success. Trade-off requirements are the requirements which are pursued as much as possible but, should they not be met, the system will still be usable to a satisfactory extent.

2.2.1. Mandatory Requirements

1. Dimensions shall not exceed 70mm x 30mm x 10mm (L x W x H) .
2. Sensor patch must be placed on the chest.
3. Must measure temperature, heart rate, oxygen saturation, bilirubin
4. The previously mentioned measurements need to be performed at least once every 2 hours.
5. Must have battery life of at least 3 days.
6. The sensor patch must be wireless.
7. It should be able to detect neonatal jaundice when the baby is at risk.
8. Be able to communicate these measurements to a hospital real-time.
9. Must be reusable.
10. Must be sterile as it will be medically used.

2.2.2. Trade-off Requirements

As the sensor patch will be worn continuously by babies for possibly three days, it is desirable to make it comfortable for the baby. This can however impact the mandatory requirements negatively like size and battery life as a smaller sensor patch would probably be more comfortable, but would limit the space for the battery and components. Making the sensor patch waterproof would make it possible for the baby to take a bath without damaging the sensor patch. It would make the design more complex and possibly negatively influence sensor accuracy. On the other hand making the device waterproof will increase life. The duration of reliable operation of the sensor is influenced by the price and availability of components and the resistance to damage. The sensor must be reliable for at least a year as this will make the sensor reusable to a high degree, however making it last longer can end up in a more expensive product. Therefor these are trade-off requirements.

1. Should be waterproof
2. The patch must provide reliable operation for one year, used on two patients per week.
3. Should not bring discomfort to the baby

2.3. Decomposition of the system

The project has been divided into three subsystems. The systems are: energy, sensors and communication and microcontroller. The system has been divided into these subsystems since they are expected to have equal weights. Besides this, each subsystem has a clear unique challenge that needs to be solved. The energy group needs to simulate the energy consumption and pick an appropriate battery. The sensor group needs to design sensors that meet a set of specific requirements. Finally, the microcontroller and communication group needs to design an efficient smart system that controls the entire system.

Energy system
The energy group focuses on everything related to energy and power within the system. Energy storage, power and energy management and visualising data with the aid of a MATLAB model are the topics and tasks of this subgroup.

Sensor system
The sensor group will design a sensor system to measure temperature, heart rate and respiration rate, oxygen saturation and bilirubin. The bilirubin sensor has to be designed since this kind of sensor is not yet available to buy off the shelf. The other measurements can be performed using already available sensors. These sensors will need to be selected based on several parameters (e.g. accuracy, energy consumption)

Microcontroller and communication system
This group will look at the implementation of a microcontroller which will act as a central processing unit for driving all actions within the system. Additionally, this group will look at different possibilities for choices of communication protocols by which the system will communicate wirelessly with the user. When a communication protocol has been chosen, this group will look at the most efficient implementation and integration with the microcontroller.

2.4. Requirements for sensor group

The main purpose of the sensors is to measure the medical status of new born infants. Several parameters which indicate the health of the infant will need to be measured. The sensors need to convert physical properties of the infant into measurable electrical signals.

Measurement data from the sensors need to be sent to the micro-controller. The timing of the measurements of the individual sensors is regulated by the micro-controller. The sensors therefore need to understand the command signals from the micro-controller too. The parameters need to be measured to an accuracy that is conform to the medical regulations (e.g. temperature measurements should not deviate more than 0.1°C).

In Table 2.1 the requirements of the sensors is shown. The sensors should be affordable, therefore the price of the individual component cannot be to high. Furthermore, the sensors should be low power due to the limited battery power. The dimensions of the sensor patch are limited since it should be placed on the chest of a newborn. Therefore, the sensors should be as small as possible. The accuracy of the sensors should be high enough to be able to replace conventional medical equipment. Finally the sensors should be able to communicate the measured data to the micro-controller.

Table 2.1: Functional requirements Sensors

	Name	**Description**
1	Price	complete sensor system should not exceed €40
2	Dimensions	double sided PCB with dimensions 2 by 3 cm and a single sided PCB with dimensions 1.5 by 1 cm.
3	Power	Sensors and supporting electrical components should use no more than 20J per day)
4	Communication	Sensors should be able to communicate with the micro-processor to receive commands to do measurements and to send measurement results
5	Measurements	Sensors should measure temperature, respiration rate, heart rate, oxygen saturation and bilirubin levels
6	Accuracy	Sensor measurements should be sufficiently accurate for medical relevance.
7	Non invasive	The sensors need to be non invasive, meaning the skin may not be pierced for measurements
8	Location	The sensors have to be placed on the chest.

3

Measuring techniques

The medical parameters that give insight in the health of the infants are non electronic signals. They therefore need to be converted to an electronic signal in order to be measurable. Sensor devices are able to convert properties of the human body from a physical to an electrical domain. The conversion can be achieved in various different ways depending upon the parameter measured. The different ways of conversion makes for different sensing techniques. In this chapter an analysis will be done to establish which sensing technique is most appropriate for measuring a certain medical parameters. The medical parameters that need to be measured are: core temperature, respiration rate, heart rate, oxygen saturation and bilirubin.

The analysis will take a few design factors into account, some are: size, accuracy, energy consumption, ease of implementation and price. The medical parameters, the sensing devices will need to measure, have been determined in 2. Only the sensors capable of detecting these parameters will be analysed.

3.1. Temperature

Measuring the temperature at the chest will give a different result from measuring internal temperature by using invasive measuring methods. There are correlations between chest temperature and internal core temperature that are accurate enough in order for non-invasive methods to be used instead of invasive methods [26]. This estimated core temperature is determined using external chest temperature, heart rate, body activity and environmental variables (humidity and ambient temperature). Heart rate and body activity (chest movements) will be measured by other sensors and can be used to estimate core temperature. Environmental variables will not be measured. Tests using a prototype without environmental variables will need to be performed to determine the need for these.

There are several means of determining temperature. The application of each temperature measuring technique is based on the advantages and disadvantages it possesses. Some devices might suit an industrial better than a medical application. Devices suited for medical use will need to be identified. Devices need to be accurate (random error deviation less than 0.1°C), small (order magnitude mm by mm), easy to implement, energy efficient and low cost.

3.1.1. Thermocouples

In a thermocouple two conductors or semiconductors with dissimilar electronical properties make contact to form an electronical junction. A voltage is induced between two contact points of different temperature. The voltage is temperature dependent due to the thermoelectric effect, therefore it is possible to measure temperature based on the voltage reading. As thermocouples induce a voltage they can be considered self powered. Thermocouples can be made out of various materials, the choice of materials give the thermocouple its properties. The main drawback of thermocouples is the lack of accuracy, accurate measurements within one degree Celsius are hard to obtain with thermocouples. A number of pros and cons have been established to determine the usability of thermocouples, see table 3.1.

Table 3.1: Pros and cons of thermocouples

Pros	**Cons**
Wide temperature range (-200°C to 2300°C)	Lack of accuracy (error larger than 1°C)
Self-powered	Expensive (approx. €10)
Fast response	Non linear
Suitable for high vibration and shock environments	Low voltage output (10-70 uV/°C)
Tip sensitive	Reference temperature required
	Extra hardware needed, increases footprint and energy use

The main reasons why thermocouples are not suitable for the purpose of this sensor system are the lack of accuracy and the need for a reference temperature. For medical reasons the error in temperature measurements should be around 0.1°C, this is not feasible using thermocouples. Furthermore, it will be hard to implement a steady known reference temperature within the small sensor system as temperatures can be influenced by surrounding temperature changes. A technique of reference-junction compensation can be implemented to overcome the problem. The reference temperature will be measured by another temperature sensing device and the thermocouple voltage reading can be adjusted using the measured reference temperature. By using another temperature sensing device the system only becomes larger, more energy use intensive and complicated, all undesired consequences. For these reasons thermocouples will not be used.

3.1.2. Resistance temperature detectors

Resistance temperature detectors (RTDs) use a well known accurate relationship between resistance and temperature of a material. The materials used are often pure forms of platinum, nickel or copper. The relationship can be used to give an accurate measure of ambient temperature. The accuracy of the temperature measurement is not only based on the predictability of the relationship between temperature and resistance but also on the accurate measurement of the resistance of the resistive element. Resistances of the leads connecting the RTD element have impact on the measurements. There are wire configurations to limit the negative effects of the lead resistances.

Thin-film, wire-wound, and coiled elements are the three most used types of resistance temperature detector sensors. These have slightly different properties making one type more suitable in a particular application than another. Thin-film detectors are composed of a ceramic substrate with an extremely thin layer of metal on top of it. The thin layer of metal is the resistive element. The stability of the thin-film is less than the stability of the other types. Wire-wound elements are composed of a thin metal wire wrapped around a core of insulating material. Wire-wound elements provide better accuracy compared to thin-film elements. Finally coiled elements are comprised of wire coils held in place by a ceramic support structure surrounding it. The coils can expand freely as temperatures increase, therefore they can be used at higher temperatures (up to 850°C). When not able to expand freely the elements may get damaged at higher temperatures. Coiled elements are widely used for industrial purposes. Thin-film elements are most suitable for wearable sensors as they can be extremely thin.

A number of pros and cons have been established to determine the usability of RTDs, see table 3.2. These pros and cons have been generalised for the different RTD types for simplicity purposes.

Table 3.2: Pros and cons of resistance temperature detectors

Pros	**Cons**
Accuracy up to 0.05°C	Expensive for high accuracy (approx. €10)
Long term stability	Constant current source required (approx. 1 mA)
Repeatable	Self-heating error
Wide temperature range (-200 to 850)	Slow response
Small variation between detectors	Not suitable for high vibration and shock environments
Relative small size (order magnitude: mm x mm)	Extra hardware needed, increases footprint and energy use

RTDs could potentially be used as the accuracy is sufficient, but it would have some practical drawbacks. To work properly RTDs need a constant current source of between 0.1 and 1 mA at the low end of the spectrum. Deviations in the output of the current source influences the accuracy of RTDs. The achievable accuracy of 0.1°C maximum deviation is under ideal circumstances. Besides being dependent upon the constant current source the accuracy is also influenced by the quality of the connection to an ADC and the quality of the ADC and complementary circuit itself. Meaning an accuracy of 0.1°C is hard to achieve. Due to the extra hardware surrounding the RTD itself the total footprint may end up coming close to 1 cm^2 making it less ideal to use. Furthermore the temperature sensor will be rather expensive at €10.

3.1.3. Thermistors

Thermistors work in a similar way to RTDs as both are resistance thermometers, the resistance is dependent on the temperature of the device. By measuring the resistance of the device the temperature can be derived using a predetermined relationship between resistance and temperature. The relationship is harder to model as opposed to RTDs it is not linear but rather exponential for thermistors. Instead of using pure forms of metal like in RTDs, thermistors are produced using metal oxides or polymers. The use of metal oxides gives thermistors a larger internal resistance and a larger change of resistance due to a change in temperature compared to RTDs. A more accurate measure of temperature can therefore be achieved as the elements are more sensitive to a change in temperature. Furthermore the overall larger resistance has as an added effect that the resistance of the connecting leads has little impact on the measurements of resistance of the thermistor as they are comparably small. This all makes thermistors highly accurate (0.05°C accurate element can be found, 0.1°C more typical) provided the relationship between resistance and temperature is properly defined. Table 3.3 provides a summary of the advantages and disadvantages.

Table 3.3: Pros and cons of thermistors

Pros	**Cons**
Fast response	Non linear characteristics
Inexpensive (1 or 2 euros)	Self heating error
Small size (SMD packages)	Unstable long-term due to drift and decalibration
High accuracy (0.1°C)	Extra hardware needed, increases footprint and energy use
High sensitivity	

Thermistors can be excellent devices to measure temperature in a wearable sensor system as they are small, inexpensive, highly sensitive and accurate. The latter is under assumption that the non linearity and self heating errors are accounted for. The negative effects of these can be minimised by accurately mapping the temperature resistance relationship and calibrating the device properly. The self heating error becomes a problem when the constant excitation current source needed to induce a measurable voltage across the thermistor is large. Smaller excitation currents decrease the dissipation power to limit the self heating effects. This has as added bonus a lower power consumption, which is important criteria to the design of the wearable sensor system. There is however also a downside to decreasing excitation current as the sensitivity will

decrease, the induced voltage is of smaller magnitude when the excitation current is smaller. These factors need to be taken into account when a complete temperature sensing device is designed.

3.1.4. Infrared sensors

Temperature sensors using infrared (IR) to measure surface temperature of objects detect thermal radiation in the form of IR light to determine the temperature. All objects with energy emit thermal radiation, also known as black-body radiation. The thermal radiation from an object is focused using a lens on to a detector. The detector produces an electrical signal dependent upon the amount of radiation power that strikes the detector. Inside the infrared sensor there are compensation algorithms to compensate for ambient temperature variations. Without these compensation algorithms measurements lack accuracy. IR sensors can detect the temperature of an object without making direct contact as thermal radiation can travel through air. IR sensors work within ranges of a couple of meters.

Table 3.4: Pros and cons of infrared sensors

Pros	**Cons**
Small size (smd packages)	Expensive (more than €10)
Medical accuracy (0.2°C)	Not designed for close ranges (few mm separation)
Measurements without direct contact	Covering device even transparent influences measurements
Fast response	Affected by humidity
	Affected by radio frequencies

Infrared sensors are not suitable for measuring temperature with a system attached to the skin. Infrared sensors are designed for use at ranges of tens of centimeters. Furthermore the sensors will need to be protected from sweat by a water resistive material. Even when this material is transparent the measurements performed by the IR sensor will be negatively affected by it. Lastly the sensors are rather expensive compared to the other techniques available for measuring temperature.

3.1.5. Semiconductors

Semiconductor temperature sensors are a type of integrated circuit i.e. IC. Like many of electronic semiconductor devices produced nowadays (e.g. microprocessors) IC temperature sensors are produced in a similar way. The semiconductors diodes used in these ICs have a voltage current relationship dependent upon the temperature of the device. If this relationship is well known for a particular semiconductor diode the temperature of the device can be determined using measurements of voltage and current of the diode. Often a very constant excitation current source is needed for this as then the voltage across the diode provides the information needed to determine the temperature. The diode is often housed together with the needed amplifiers, ADCs, signal processing hardware, compensation hardware, digital communication logic (e.g. I2C or SPI), etc. to form an all-in-one device. This makes the device rather easy to use. The output of the entire device is a digital representation of the measured temperature, no external signal processing software needed to derive the temperature.

Table 3.5: Pros and cons of semiconductor devices

Pros	Cons
Cheap	Temperature sensitive element covered by housing
small size (smd packages)	Accuracy best around calibration point
High accuracy (up to 0.05°C)	May contain unnecessary design options
Easy to use (internal ADC and I2C interface)	
Linear behaviour	
Output needs no data processing	
Low power use	

Semiconductor temperature sensing devices are well suited in a wearable sensor system as they are small, low power, accurate, cheap and can directly communicate with a microprocessor without needing any additional hardware. The only issue with these type of devices is that the diode, the temperature sensitive element, is enclosed in a housing and cannot make direct contact with the surface of the object that is of interest for temperature measurements. The error will be small as the entire device is small and has a low thermal mass and can be compensated by a microprocessor, if present. The devices are most accurate around the calibration point, moving further form these point the accuracy decreases. For a lot of applications the narrow temperature range where the device is accurate is a drawback. However as the device will measure body surface temperature ranging between 33 and 37 °C an IC temperature sensor with a calibration point around this range will experience no problems with lack of accuracy. The devices contain all the necessary hardware and software to make the temperature measurements possible. The manufacturer has left some design choices regarding for example sample rate, sensitivity, modes of operation, etc. to the user. Changing the value of internal registers alters the behaviour of the sensor. This also leaves unnecessary functionality (e.g. making an interrupt pin high when a threshold temperature has been achieved) to use energy. Even with the added hardware the energy usage is very low, around 100uA for active conversion time and 200nA for standby/shutdown time.

3.1.6. Conclusion

When considering the application of being used in a wearable sensing device there are two techniques that are best suited for this purpose, these are the thermistors and the semiconductor temperature sensors. As they are the most accurate, cheapest and smallest compared to the other techniques and experience hardly any major draw backs. Both do have slight systematic measurement errors. Thermistors can be affected by self heating phenomena and semiconductor temperature sensors are not in direct contact with the measured object. these slight problems can be minimised or compensated for and should not be of major concern.

When comparing thermistors with semiconductor devices, thermistors require surrounding supporting hardware while semiconductor devices come in in all-in-one package. the supporting hardware requires a longer design process and uses more space. Thermistors can however be better optimised for a certain purpose, while the all-in-one packages might need to make trade-offs to make them useful in a broad application spectrum and may contain superfluous hardware only needed in certain applications.

With semiconductor devices fulfilling all requirements there is no need to make a more optimised design using thermistors. Furthermore the ease of use of semiconductor temperature sensors is a major advantage for this particular sensor system as more time and PCB space can be utilised in designing the other sensors. Furthermore being able to communicate directly with a microprocessor using I2C or SPI makes semiconductor devices very attractive. So to conclude semiconductor devices will be used in the sensor system to measure temperature.

3.2. Respiration rate

There are many contact-based methods for measuring respiration rate, these are all noninvasive. These methods are all performed in either the region of the mouth or the chest [13]. As the sensor patch will be placed in the chest area, these methods will be explored further.

3.2.1. Acoustic measurements

Microphones can be used to measure the sound produced by air passing through the throat and airways of the patient. Microphones are transducers that can produce electrical signals from acoustic pressure variations. There are various different typologies for enabling the conversion. microphones can use capacitors, electrets, moving-coils, piezoelectric elements or even fiber optics to detect differences in acoustic pressures. The most common method employs capacitors. The output of the sensing device needs to be amplified, filtered and eventually digitalized using an ADC.

The major drawback of a microphone based approach is the high influence of noise from either the environment or the subject itself. In the case of the sensor patch the sounds of parents, toys and crying can make accurately measuring the respiration rate almost impossible. It can partially be overcome by implementing noise-robust algorithms. However they require large amounts of signal processing techniques and are therefore often not used when compared to other methods. Microphones should only be used in extremely low noise and structured environments (e.g.,Intensive care departments of hospitals).

3.2.2. Chest wall movements

Breathing causing contraction (breathing out) and expansion (breathing in) the chest wall. Measuring chest wall movements is for this reason a good method for determining respiration rate. The movements of the chest can be measured using various techniques. There are three main approaches: measuring chest wall strain caused by respiratory activity, measuring transthoracic impedance changes and measuring the movements of the thorax in three dimensions.

Strain measurements

Strain sensors measure the deformation of the the chest to determine the respiratory activity. the sensors work on several methods, but all have the aim to measure the cyclic expansion and contraction of the chest. Some of these methods are: resistive sensors, capacitive sensors and inductive sensors

Resistive sensors use piezo-resistive sensing elements. the resistance of these elements changes with the shape of the element. The resistance is related to the strain and thus cyclic chest movements. Often piezoresistive elements are implemented in a textile-based products. There are two main drawbacks: The durability of the sensing elements is low and thus not ideal when aiming for repeatability and the sensors are affected by all movements not only respiratory induced movements.

Capacitive sensors are comprised of two electrodes placed on either side of the chest. The electrodes measure the change in capacitance of the chest during breathing. When breathing both the distance between electrodes and the permittivity changes. These factors influence the capacitance of the chest. The permittivity changes as air with a lower permittivity enters the body during breathing. Capacitive sensors produce accurate and reliable results when multiple electrodes are used. The major down side of this method is the large size. The components are not of large size, but the electrodes need to be placed on either sides of the chest. This makes the sensor large and requires wires.

Inductive sensor systems measure the change in self-inductance and oscillating frequency of coils placed around the rib cage and abdomen during breathing. The inductive sensing method has been widely used in commercial products as these sensors achieve good levels of accuracy and repeatability. However the method requires coils around the upper body making it large and potentially uncomfortable.

Transthoracic impedance measurements

The conductivity of the chest changes during breathing. Breathing air in lowers the overall conductivity as air is a poor conductor when compared to body fluids. Furthermore, the conductance paths increase in length as the chest expands. These influences on the conductivity can be measured using electrodes. There are two pairs of electrodes, one pair induces a low-amplitude current (< 1 mA) with a high frequency (50 kHz). The other pair measures voltage differences between the two electrodes giving a measure of impedance. The number of electrodes and the requirement of placing the electrodes evenly distributed around the chest area gives this method a large footprint and the need for wires. This can be considered the largest drawback.

Movement measurements

The three dimensional movements of the chest can be measured to determine the respiration rate. The movements of the chest change acceleration forces, angular velocities and magnetic field. These three parameters can be measured using accelerometers, gyroscopes and magnetometers respectively.

Accelerometers measure the acceleration the device experiences in three directions (x,y,z). depending on the placement of the chest one of the axis will show more dominantly than the other axis the forward movement of the chest.

Gyroscpes measure rotation of the device around either 1,2 or 3 axis. They may produce a divergent output due to sensor drift [17]. Usually a accelerometer is used in combination with the gyroscope to overcome this.

Magnetometers record the changes in magnetic fields due to movement of the device. A magnet is used as a source of the magnetic field. Magnetometers are highly sensitive devices and can potentially accurately detect chest movements, however they also are highly sensitive to other body movements and to external alterations of the magnetic field, present in unsuitable environments.

All three sensing methods are highly sensitive and small (MEMS technology), however they are all susceptible to body movement, not just related to breathing. Filtering algorithms can be used to remove other bodily movements [24].

3.2.3. Modulation cardiac activity

From data containing cardiac activity a modulation scheme can be used to extract information regarding respiration activity. There are two heart monitoring sensors methods that can support the modulation algorithms: Electrocardiography (ECG) and photoplethysmographic (PPG) sensors.

ECG, described in greater detail in section 3.3.2, uses electrodes to measure the electrical activity of the heart muscles. ECG system can be expensive and are influenced by body movement and environmental changes, but less sensitive than devices that measure chest movements. As ECG uses electrodes there is again a problem regarding the presence of wires and the large space between electrodes.

PPG, described in greater detail in section **??**, uses different wavelength light emitted from LEDs to estimate concentration of blood components in pulsatile blood as the light travels through the skin. The reflected light from the skin is measured by a photo diode and the output signal contains information regarding blood properties and heart rate. PPG sensors are cheap and small sized. PPG is sensitive to body movements and these can impact the accuracy of the measured heart rate obtained from modulating the PPG sensor data.

Both these methods can work presuming the data from the ECG and PPG sensors are accurate. When the data from the ECG and PPG sensors contains errors the extracted respiration rate due to modulation also contains errors.

3.2.4. Conclusion

Table 3.6 summarizes all the sensors mentioned. Accelerometers, gyroscopes and microphones can be considered best suited for the use in the sensor system to measure respiration rate, but they all have a major drawbacks which need consideration. The measurements of the microphone are easily influenced by all sounds not originating from the respiration activity. These are hard to filter out using noise reducing algorithms as for instances voices or crying are far louder than the feint noise of respiration. Accelerometers and gyroscopes are very sensitive to body movements and measurements can be disrupted easily. However in contrary to noise reduction algorithms, filtering other body movements from chest movements is more easily achieved. This is especially true for the accelerometer as chest movements are predominantly present in one axis, while body movements will affect all axis and thus the possibility of differentiating between chest movements and body movements can be made. The accelerometer will be used in the sensor system to measure chest respiration.

Table 3.6: List of sensors able to measure respiration rate with scores for some properties and characteristics

Sensor	Size	Wires	Cost	Sensitivity to body movements	Influenced by environment
Microphones	+	+	+	+	–
Strain Sensors					
Resistive				-	
Capacitive	-	-		-	+
Inductive	–				+
Transthoracic impedance	-	-		-	+
Movement					
Accelerometers	++	+	+	-	+
Gyroscopes	++	+	+	-	+
Magnetometers	++	+	+	-	-
Modulation					
ECG	-	-	-		
PPG	+	+		-	+

3.3. Heart rate

There are many different methods to detect the heart rate. The requirements of the heart rate sensor is that it has to be accurate, low noise, low power and small. In this section some noninvasive methods will be explained and their advantages and disadvantages will be discussed. .

3.3.1. Dielectric plethysmography

DPG measures the change in permittivity of the tissue caused by the expansion and contraction of the arteries. This change in permittivity can be sensed in multiple ways. Chien [6] uses the changes in the tissue dielectric property is measured by using gigahertz-frequency fringing electric fields. The gigahertz-frequency is chosen to take advantage of the dielectric contrast between the pulsing blood flow and the surrounding tissue in the gigahertz frequency band. Another method for heart rate measurements using dielectric plethysmography is using is used by Jovanov [15]. Here the change in permittivity is measured using a capacitive sensor. The advantages of these methods are that the signal obtained from this signal is not sensitive to skin tones. Furthermore, these methods are more power efficient than optical measurements since no power is lost due to light absorption or scattering in the tissue. However, these methods are more sensitive to motion and the proposed sensors are not yet available for purchase.

3.3.2. ECG

ECG stands for electrocardiography and this method is based on detecting the electrical signals of the heart. During the contraction or relaxation of the heart cells, electrical depolarization and re-polarization occurs. This process generates surface potentials which can be detected by electrodes. The delay between the depolarization and re-polarization of different regions in the heart results in the typical ECG graph which is shown in the top half of Figure 3.1 from [18].

Typically the timing between two consecutive heartbeats is the distance between two R-wave peaks. The advantage of this technique is that it can be very low power. However, since reducing inter electrode distance will decrease signal strength [23], the ecg sensor would have to be relatively large in order to get an accurate measurement.

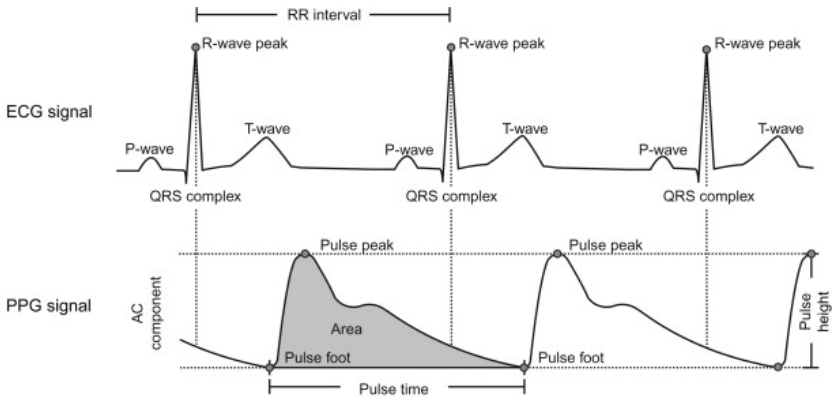

Figure 3.1: ECG and PPG graph

3.3.3. PPG

PPG stands for Photoplethysmography. It uses a light source which emits light at the tissue's surface. Thereafter a photodiode measures the intensity of the reflected non absorbed light. With these measurements the volumetric variation in the blood can be obtained. In the bottom of Figure 3.1 a typical PPG signal is shown. The advantages of using this method are that it is relatively simple in operation and the technology is inexpensive. However, the accuracy of this method decreases when the patient moves or is exercising. Furthermore, PPG has a relatively higher power consumption due to the light scattering in the tissue.

3.3.4. Phonocardiography

Heart rate can also be detected with the help of microphones by listening to the sounds of the heart and recording acoustic signals produced by the human cardiovascular and bronchopulmonary systems but also conducting a mathematical analysis of these sounds in order to compose an objective conclusion on patients' state of health. In [34] various possible types of devices are discussed:

- Dynamic Microphone: This is the most common type of microphone. It consists of a membrane attached to a copper coil. This coil is placed in an electric field. Therefore, when the membrane vibrates due to sound pressure,the coil will move around in the electric field which will result in induction. The sensitivity of this microphone is from 1 mV/Pa. Furthermore, the frequency range is from 10-50Hz to 10-15kHz. The advantage of a dynamic micro-phone is that it has a very low noise level. However, the sensitivity is relatively low and the construction is quite large
- Condenser microphone: This microphone consists of a metallized polymer film. This film carries a voltage. When the film vibrates due to sound it creates low frequency signals. Another type of this microphone is called an electret microphone. The advantage of this microphone is that no external voltage source is needed since at the creation of the electret a electrostatic charge is formed. This kind has a sensitivity of 1.5 mV/Pa. However, the output impedance of this kind of microphones is quite large.
- Piezoelectric microphone: This kind of microphone consists of a piezoelectric material which potential changes as a result of sound pressure. This kind of microphones have an extremely high sensitivity up to 50 mV/Pa. However, in order to operate correctly a good contact with the skin is needed. According to Zhdanov et al, these kind of sensors are the most preferable for detecting heart rate sounds.
- Mems microphone: MEMS microphones are microphones which are built using the MEMS technology. Therefore, these microphones can be really small. They have less noise than the other microphones discussed earlier. In the comparison performed in [34] this type had the best quality of bronchopulmonary sounds.

3.3.5. Conclusion

In this section several heart rate measurement methods were discussed. The DPG method has a low power consumption and is not sensitive for different skin tones. However, the design of this kind of sensor is more complex than for the other methods mentioned in this section The ECG method is still the golden standard

in the medical field. However, an ECG sensor needs at least two electrodes and these electrodes need to be placed at a significant distance from each other, which would make the sensor relatively large. Detecting the heart rate using phonography is another option discussed in this section. The disadvantage of these kind of sensor is that it is quite sensitive to moist and temperature. The final method is PPG which has the advantage of being a simple and inexpensive technology. Furthermore, by using this technology the oxygen saturation can be detected at the same time which removes the need for another separate sensor. For these reasons the PPG technology has been chosen for the sensor patch.

3.4. Oxygen saturation

Oxygen saturation is another vital health parameter that needs to be measured. Oxygen saturation is the ratio of the total hemoglobin concentration and the concentration of hemoglobin with bound oxygen atoms, see Equation 3.1.

$$S = \frac{O_2Hb}{O_2Hb + RHb} \tag{3.1}$$

The most common noninvasive way of measuring oxygen saturation is by using pulse oximetry. Pulse oximetry is based on PPG, see Section 3.3.3, and uses the difference in light absorption between hemoglobin and oxyhemoglobin. A typical pulse oximeter uses two leds. One red led with a wavelength around 645 nm and one infrared led with a wavelength of 940 nm, since the absorption of light differs significantly at these wavelength between hemoglobin and oxyhemoglobin. The reflected light is thereafter collected by a photodiode. The amplitude of the PPG wave signal is commonly denoted as AC and the baseline is denoted as DC. For Pulse oximetry the only relevant information is in relative change of amplitude of the PPG waves. Therefore, the ratio between the absorbance of red and infra led is shown in 3.2.

$$R = \frac{AC_{red}/DC_{red}}{AC_{IR}/DC_{IR}} \tag{3.2}$$

In order to determine the oxygen saturation from the obtained ratio, a calibration curve should be empirically generated by measuring the ratio in healthy patients with different levels of oxygen saturation. Thereafter, the microprocessor can link the ratio calculated in 3.2 to a level of oxygen saturation.

3.5. Bilirubin

Jaundice is a common illness for neonates. Jaundice is caused by an increased level of a substance called bilirubin, which causes a yellow discoloration of the skin . This substance is made when red blood cells are broken down. Normally the liver will remove bilirubin but the liver of a neonate is often too immature to perform this task. This condition is common for neonates in their first week. However, severe neonatal jaundice can occur if the neonates are not monitored and treated in a timely fashion. Severe neonatal jaundice can result in deafness and brain damage.

Normally the severity of neonatal jaundice is assessed by visual examination by doctors. However, due to the subjective nature of this kind of assessment the reliability is questionable. In order to quantify the bilirubin concentration serological tests are usually performed. These tests are performed by taking blood samples from the neonates which is an invasive procedure which should be avoided when possible.

The principle behind the detection of bilirubin in the blood is the difference in light absorption between bilirubin and the other blood components. In Figure 3.2 the absorption coefficients of bilirubin, hemoglobin and oxyhemoglobin are plotted against wavelength.

As can be seen from the Figure, at wavelengths between 460 nm and 480 nm the molar attenuation coefficient of bilirubin is significantly higher than that of hemoglobin. Therefore, the same principle as used in PPG (see Section 3.3.3) can be applied for the bilirubin sensor. In [16] the diffuse reflectance of the neonates skin was simulated using Monte Carlo simulations. With these simulations absorption, reflection and transmission can be simulated. These simulations result in a different reflectance spectra for different values of bilirubin, melanin and blood concentrations. From these simulations is concluded that between the wavelengths of 400 and 520 nm the bilirubin concentration variance has the most influence on the diffuse reflectance. This is inline with what is shown in Figure 3.2. Hemoglobin does not have much influence on the diffuse reflectance between these wavelength. However, melanin has a major influence on the reflectance over the whole spectrum therefore it is important that the effect of melanin is eliminated. This is achieved by noticing

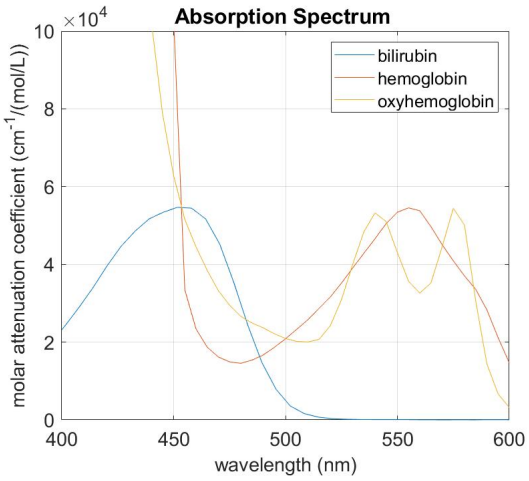

Figure 3.2: Absorption spectrum blood

that there is a band between 600 and 700 nm where the reflectance varies highly with the melanin concentration. This means that from the obtained measurements the melanin components can easily be subtracted.

In order to obtain an accurate bilirubin concentration, calibration is needed. This calibration would have to be performed by measuring the bilirubin concentration with a clinical certified device and thereafter comparing the results with the results of the designed device and find correlation between the two measurements. The design of the bilirubin sensor is discussed in Chapter 5.

3.6. conclusion

At the start of the chapter it was stated that the following medical parameters have to be measured by the system: core temperature, respiration rate, heart rate, oxygen saturation and bilirubin. In this chapter several methods for obtaining these were explored. Eventually some methods were selected that will be used for further design processes. Core temperature will be measured using semiconductor devices. Acceleration sensors will be used to measure respiration rate. Finally the decision was made to design one PPG sensor capable of measuring the remaining medical parameters.

4

Choice of sensors

In this chapter sensing devices will be chosen based on the previous chapter, chapter 3, exploring the different ways in which temperature, respiration rate, heart rate, oxygen saturation and bilirubin can be measured. It will take into account the restriction and requirements made in chapter 2 (e.g. accuracy, energy consumption, size, price).

4.1. Temperature sensor

In section 3.1 different methods for determining the temperature were explored in order to understand which technique was best suited for temperature monitoring at a medical level using a small sensor system. Leading to the conclusion that semiconductor temperature sensing devices were best suited. In the following section the requirements for the temperature sensor will be clearly defined. Using these requirements, analyses regarding these parameter will be performed to obtain understanding of the best performing sensor.

4.1.1. Design requirements

Previously some factors (e.g.,accuracy, size, energy efficiency) have been mentioned in section 3.1, which give insight in the quality of sensors and if they are an appropriate choice for the project. These design requirements need to be specified more precisely in order to determine if a particular sensor fulfills the requirements. There are six important design requirements, given in table 4.1, that need to be considered. The requirements are in order of importance.

Table 4.1: Design requirements for selecting a temperature sensor

Design requirement	**Requirement specification**
Accuracy	The measured surface temperature and actual surface temperature may not differ more than 0.1°C. Systematic errors are not considered as these can be removed using calibration.
Temperature range	The sensor accuracy needs to hold for the temperature range of 30 to 40°C. Surface temperature of the skin will have a value within this range.
Energy consumption	Sensors may not use more than 0.3J of energy per day.
Measure frequency	The temperature needs to be measured at a minimum of once per two hours. This may be increased to improve accuracy (using averaging) as long as the energy consumption requirement is not violated.
Size	Sensors need to be as small as possible without sacrificing accuracy and energy consumption, Temperature sensor may not be larger than 5 by 5 mm.
Price	Temperature sensors may not exceed a price of €3.

4.1.2. Analysis of a selection of sensors

A selection of sensors were selected for the comparison between them to find the sensors that fit the design requirements the best. All these sensors claimed to be accurate, low power and small in size. Furthermore, all had an I2C interface for ease of implementation and communication with a microcontroller. The selection is comprised of the following eight temperature sensors: TMP117, TMP102, STTS751, MCP9808, MAX30208, MAX30205, AS6212 and Si7051. The sensors will first receive an analysis to determine their potential accuracy as it has to fulfill this requirement.

Accuracy

In the design requirements it was established accuracy is a very important criteria and measured temperature needs to be within 0.1°C degree maximum deviation from the actual skin temperature. The level of accuracy needs to be reached in the temperature range of 30 tot 40°C. Information regarding the accuracy of the selection of sensors was extracted from their datasheets. These gave information about the minimum, typical and maximum deviations in temperature reading at a given temperature range. Some of these temperature ranges are very large and the datasheets do not give information on the accuracy from 30 to 40°C, which may have a better accuracy within this range as it could be closer to a calibration point. But assumptions about the accuracy within the temperature range, of interest for this application, cannot be made. Table 4.2 shows the quality of measurements for the various sensors.

Table 4.2: Accuracy analysis of temperature sensors

Sensor	**Accuracy (deviation in °C)**			**Temperature range (°C)**
	MIN	TYP	MAX	
TMP117	-0.1	0.05	0.1	-20 < T < 55
TMP102	-2	±0.5	2	-25 < T < 85
STTS751	-1.5	±0.5	1.5	0 < T < 85
MCP9808	-0.5	±0.25	0.5	-20 < T < 100
MAX30208	-0.1	±0.1	0.1	30 < T < 50
MAX30205	-0.1	±0.1	0.1	37 < T < 39
	-0.2	±0.2	0.2	35.8 < T < 41
	-0.3	±0.3	0.3	15 < T < 45
AS6212	-0.2	±0.2	0.2	-10 < T < 65
Si7051	-0.1	±0.1	0.1	35.8 < T < 41
	-0.13	±0.13	0.13	20 < T < 70

From the table it is clear that the TMP117, MAX30208, AS6212, Si7051 are usable sensors when considering accuracy. The AS6212 sensor is actually not accurate enough when performing single measurements. However, by taking multiple measurements and averaging the results, the accuracy can be improved to meet the design requirements. This only holds if the error between measured temperature and actual temperature is a random error and not a systematic error. Averaging may consume more energy as more measurements need to be performed. In the analysis regarding energy consumption of the sensors, the effect of increasing the number of measurement on the energy consumed will be determined.

Energy consumption

As only the TMP117, MAX30208, AS6212, Si7051 are usable sensors when considering accuracy only these will be analysed regarding their energy consumption. The sensors usually have two modes off operation. The first is the active conversion mode, also known as the measuring mode. The second mode is the standby or shutdown, depending on the sensor. In standby or shutdown mode only the I2C interface is active and thus only communication with a microcontroller is possible, the rest of the hardware inside the sensor is powered down.

Using the datasheets the power use of these modes is determined, these values will be used in the energy analysis. The voltage specified by the datasheet - used to determine the electrical characteristics by the manufacturer - was used as the voltage to determine power consumption. The power consumption in the two modes are shown in table 4.3. To calculate energy consumption, the time that the sensor spends in each mode is needed. The datasheets give the time that the sensor spends in measuring mode, this is known as the active conversion time. These times are also given in table 4.3.

Table 4.3: Energy analysis of temperature sensors.

Sensor	**Power (uW)**		**Conversion time (ms)**
	Measuring	Standby/shutdown	
TMP117	445.5	0.5	15.5
MAX30208	120.6	0.9	15
AS6212	120	0.3	36
Si7051	252	0.17	7

Using the conversion times and power usage, an estimation of the energy usage can be made. A simple Matlab script was used to make figure 4.1. The figure shows the energy consumption per hour as a function of the amount of single temperature measurements done per hour. Doing multiple measurements per hour and taking the average of these to obtain one more accurate measurement can be useful as energy consumption hardly increases with an increasing number of samples taken per hour. Averaging can improve the effect of random errors by using a series of measurements. However, systematic errors can not be removed and can only be overcome using calibration methods.

Temperature sensor Si7051 is the most energy efficient of the four tested sensors. Taking 20 measurements per hour using the Si7051 is more efficient than taking a single measurement using the other sensors. As the Si7051 can take so many measurements using little energy, it is ideal for making a single measurement per hour. Furthermore, it is more accurate than the other sensors when utilizing averaging of multiple individual measurements. When taking 20 measurements per hour the Si7051 uses around 15mJ per day, less than the design requirement of 0.3J per day.

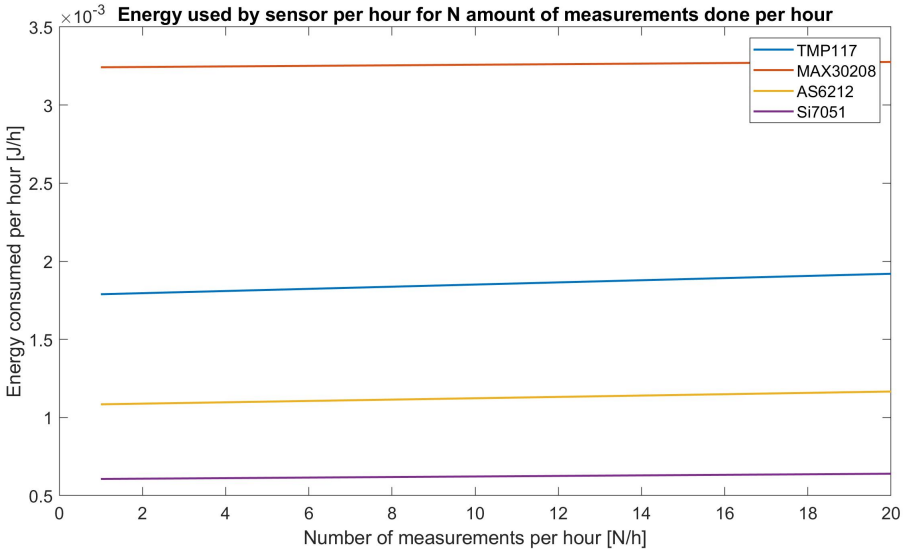

Figure 4.1: Energy consumption in joules per hour of a number of temperature sensors for different amounts of measurements per hour.

Size

All sensors in table 4.2 range in size between 1.6 x 1.6 mm and 3 x 3 mm. When taking a margin for supporting hardware (e.g. decoupling capacitors), all sensors should be 5 x 5 mm or smaller. Therefor, all sensors fulfill

the size requirement stated in table 4.1. Size will for this reason not play an as important role as accuracy and energy consumption.

Price
Of all sensors in table 4.2, the TMP117 is the most expensive at €3,38 and the least expensive is the STTS751 at €0,81. The other sensors are somewhere in the middle. Adding components like decoupling capacitors and pull-up resistors for the I2C bus, may increase the price by no more than €1, when buying top off the line components. The Si7051, which outperformed the other sensors on accuracy and energy consumption, has a price tag of €1,76. Making it sit in the middle of all temperature sensors regarding price. Together with the costs of supporting architecture the price does not exceed €3, meaning the price requirement is met.

Conclusion temperature sensor
The temperature sensor Si7051, designed and produced by Silicon Labs, fulfills all the design requirements. It outperforms all sensors on energy use by a long run. Furthermore, by measuring 9 individual times and taking the average also makes it the most accurate of the sensors, as the accuracy improves by the square of the amount of averaged samples. In this case an improvement by a factor 3 is made. This gives the Si7051 a theoretical maximum deviation between measured skin temperature and actual skin temperature of less than 0.05 °C. Being within the temperature range of 30 to 40 °C, as required. The other sensors can only manage 0.1 °C. The other sensors can also use averaging to improve their temperature deviations. However, this will increase the energy consumption to a level higher than was set in the requirements (table 4.1. Therefor, they are unable to use this method, making the Si7051 the most accurate and energy efficient.

Adding the dimensions of the supporting architecture to the footprint of the Si7051 gives it a surface area of around 5 x 3 mm and a height of 0.8 mm, within spec. Furthermore, the price of all the components for a working sensor is around €2,80, also within the set requirements.

The Si7051 uses I2C to communicate with a microprocessor. The measured temperature is represented by a series of 14 bits with a resolution of 0.01 °C. There is a correlation between skin temperature at the chest and internal core temperature [26]. Heart rate and chest movements are used for the correlation model and enable noninvasive methods to replace invasive methods to monitor patient core temperature. Implementing such an algorithm can give accurate temperature measurements.

4.2. Respiration rate sensor
In chapter 3 the choice was made to use an acceleration sensor to measure respiration rate. Based on the design requirements for the entire system the best suited sensor will be selected.

4.2.1. Design requirements

Table 4.4: Design requirements for selecting an acceleration sensor

Design requirement	Requirement specification
Sensitivity	Sensor needs to be able to detect chest movements associated with breathing
Energy consumption	Sensor may not use more than 1J of energy per day.
Measure frequency	Sensor needs to be measured at a minimum of once per two hours.
Size	Sensor needs to be as small as possible without sacrificing accuracy and energy consumption, may not be larger than 5 by 5 mm.
Price	Sensors may not exceed a price of €5.

4.2.2. Analysis selection of sensors
Several sensors were found and will be compared to find the best suited for this application. The following sensors all claimed to be accurate and low power: LIS3DH, MMA8491Q, ADXL363, ADXL362, ADXL345, BMA423, BMA456, BMA280, LIS2DS12 and IIS2DLPC. All these sensors are able to sample at 400 Hz or more, this is more than enough to do accurate measurements of acceleration to determine respiration rates. This is because breathing is a slow movement and happens at a frequency of less than 1 Hz.

Accuracy
Breathing by adults induces an acceleration of around 10 mg [14]. For newborns this will be lower. No papers could be found giving an exact acceleration number for newborn breathing. As an assumption an acceleration of 2 mg was taken. An acceleration sensor with a resolution high enough to detect the low acceleration values is needed. Studies using an acceleration sensor to measure respiration rate obtained accurate measurements using an accelerometer with a acceleration resolution of 0.2mg or less [24] [3].

Of the selection of sensors made at the start of this section, the following sensors have a resolution of approximately 0.2 mg or less: BMA456, BMA280, LIS2DS12 and IIS2DLPC. Coincidentally, these have the lowest output noise (110 - 120 ug$\sqrt{Hz}$). The output of the sensor will be filtered, rejecting all frequencies above 1 Hz as respiration rate is typically less than 60 times per minute. Total output noise will therefor be between 110 and 120 ug using the four sensors mentioned above. The IIS2DLPC has the lowest output noise of 110 ug.

Energy consumption
As only the sensors BMA456, BMA280, LIS2DS12 and IIS2DLPC are theoretically accurate enough to measure respiration rate only these sensors will receive a energy consumption analyses. Table 4.5 shows the information regarding current draw in measurement mode and standby/shutdown mode from the datasheets of the components. Furthermore the operating voltage used to perform the current measurements can be found in the table.

Table 4.5: current analysis of accelerometers

Sensor	**Average current (uA)**		**Typical operating voltage (V)**
	Measuring (@400 Hz)	Standby/shutdown	
BMA456	80	3.5	1.8
BMA280	130	2.1	2.4
LIS2DS12	150	0.7	1.8
IIS2DLPC	90	0.05	1.8

Accelerometer BMA456 and IIS2DLPC have the lowest current draw during measurements compared to the other two. However, the BMA456 consumes a lot more current when in standby compared to the BMA456. The LIS2DS12 also has a lower standby current draw than the BMA456 and BMA280, but is still far greater than that of the IIS2DLPC. The IIS2DLPC will have the lowest energy consumption of the four sensors analysed.

Each respiration rate measurement lasts 15 seconds as in this period multiple breaths can be observed, improving accuracy. The energy consumption for these 15 seconds for the II2S2DLPC will be 2.43 mJ. For the time the sensor spends in standby mode the energy consumption is 0.33 mJ per hour. Totalling 67 mJ per day, when performing a respiration rate measurement every hour. For comparison the BMA456 uses 580 mJ/day, the BMA280 uses 544 mJ/day and the LIS2DS12 uses 206 mJ/day the per day. All sensors use less than 1J per day and fulfill the energy consumption design requirements stated in table 4.4.

Size
All the acceleration sensors mentioned at the start of the section range in size between 3 x 5 mm and 2 x 2 mm. The sensors BMA456, BMA280, LIS2DS12 and IIS2DLPC which are theoretically accurate enough to measure respiration rate and fulfill the energy consumption requirements are all 2 x 2 mm and are thus the smallest of all the acceleration sensors. When taking a margin for supporting hardware (e.g., decoupling capacitors) these sensors should be 4 x 5 mm or smaller. Therefor, these sensors fulfill the size requirement stated in table 4.4.

Price
The prices of the BMA456, BMA280, LIS2DS12 and IIS2DLPC are €2,44, €2,19, €1,40 and €2,03 respectively. When considering that the supporting hardware (i.e., decoupling capacitors) will cost somewhere around €1,

the price of the entire acceleration sensor does not exceed €3,44 for the sensors. Therefor, these sensors fulfill the price requirement stated in table 4.4.

Conclusion respiration rate sensor
The acceleration sensors BMA456, BMA280, LIS2DS12 and IIS2DLPC all fulfill the design requirements in table 4.4. The only slight differences between the sensors are that the IIS2DLPC has a lower noise output and uses less energy. Furthermore the LIS2DS12 is the cheapest. The IIS2DLPC will be used for the sensor system for the reasons mentioned above and accuracy and energy use are deemed more important than costs.

The data from the IIS2DLPC is a real time measure of movement of the sensors. Algorithms to distinguish between chest movements and other body movements due to respiration have to be implemented. These algorithms exist and have been proven to be accurate to within a couple beats per minute [12]. To improve accuracy if needed a combination of accelerometers, gyroscopes and magnetometers can be used.

4.3. PPG

As mentioned in chapter 3 both the heart rate sensor and the oxygen saturation sensor will use PPG. In [19] it is shown that a PPG sensor can measure the heart rate and oxygen saturation can a be accurately when attached to the chest. The heart rate sensor only needs one LED and a photodiode. The oxygen saturation uses two LEDs, one red and one infra red, and a photodiode. Therefore, these two sensor can be combined into one sensor consisting of 2 LEDs and one photodiode. By combining the two sensors the area needed is significantly reduced. Furthermore, the bilirubin sensor will be using PPG as well since the sensor will be using the difference in light absorption between bilirubin and the rest of the blood components. The design of this sensor is discussed in Chapter 5.

4.4. Conclusion

For the temperature sensor the Si7051 has been chosen to do the temperature measurements. The IIS2DLPC acceleration sensor will perform measurements to determine respiration rate. Both these sensors have fulfilled the design requirements for the temperature and respiration rate sensors.

For the heart rate, oxygen saturation and bilirubin measurements a PPG sensor will be designed to measure them all at once. This will potentially save space and energy doing it all in one sensor.

5

Design of Photoplethysmography Sensor

As mentioned in section 4.3 the choice has been made to perform heart rate, oxygen saturation and bilirubin measurements using one PPG sensor. This chapter will describe the design process that was done to obtain a theoretical working PPG sensor. No measurements could be performed as no prototype could be made due to the situation regarding COVID-19. The design is based on theoretical models.

5.1. Design Requirements

The PPG sensor has to be able to measure the heart rate, oxygen saturation and bilirubin concentration when attached to the chest. As discussed in chapter 3, the sensor has to emit light at three different wavelengths, 645nm and 940nm for the heart rate and oxygen saturation and 470nm for the bilirubin concentration. The sensor needs to operate with a maximal voltage of 5V and a peak current of 50 mA, as small batteries for wearable devices have low output ratings. The price requirement for the entire sensor system was €40, the temperature and respiration sensor cost around €10, therefor no more than €30 may be spent on components. Similar approach was taken for determining maximum energy consumption for PPG sensor. A total energy budget of 20J was available, approximately 1.5J is used by the temperature and acceleration sensor. 18.5J can be used for PPG measurements. All design requirements for the PPG sensor can be found in table 5.1.

Table 5.1: Design requirements for PPG sensor

Design requirement	**Requirement specification**
Measurements	Measure the heart rate, oxygen saturation and bilirubin concentration
Accuracy	Measured values may not deviate more than 5% of the actual value.
Energy consumption	Sensor may not use more than 18.5J of energy per day.
Measure frequency	Measurements need to be performed at a minimum of once per two hours.
Size	Sensor may not be larger than 2 by 3 cm.
Price	Sensors may not exceed a price of €30.
Current	Sensor may not draw more than 50 mA over a period of 10 seconds, peak currents may be higher
Voltage	Sensor may not operate at a voltage higher than 5V
Location	Measurements need to be performed on the chest area.
Compatibility	Sensor must be compatible with the microprocessor (MSP430FR5994) used to control the entire system

5.2. Sensor Design

5.2.1. Black box model

The photoplethysmography sensor has several inputs and outputs and is connected to a power supply and a microcontroller (MCU). The in- and outputs are visualized in figure 5.1. The GPIO pins of the MCU are used

as inputs to control the light emitting elements of the PPG sensor. The PPG sensor radiates light into the skin of the patient. A part of the light is reflected and is collected by the sensor and transformed into an electrical signal. The output of the sensor will be fed into the MCU for signal processing and data transmission.

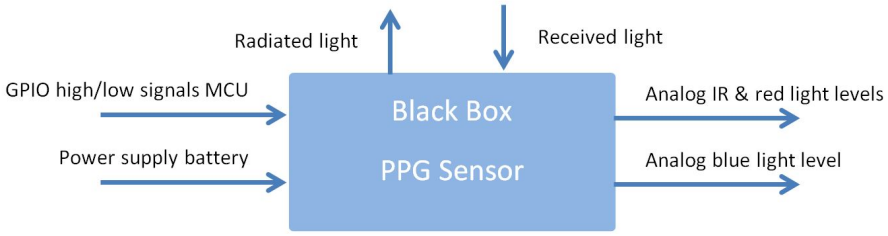

Figure 5.1: Black box model photoplethysmography sensor

The GPIO pins can have either a high of low voltage as its output, to control the PPG sensor. The voltage levels are dependent upon the supply voltage of the MCU. The MCU used is the MSP430FR5994. The MCU will be powered with a $V_{cc} = 2.0V$, this will mean according to the datasheet [] the high voltage V_{OH} of the digital outputs will range between $V_{cc} - 0.25V$ and V_{cc}. On the other hand the low voltage V_{OL} will range between $V_{ss}V$ and $V_{ss} + 0.25V$. V_{ss} is the ground connection and thus $0V$. The digital outputs can deliver a maximum current of $1mA$.

Furthermore, the MCU has 16 12 bit ADCs which can be used to convert the analog signals from the PPG sensor into digital signals. Digital signals are better suited for reliable wireless transmission. The maximum voltage range of the input of the ADC is between $0V$ and V_{cc}, $V_{cc} = 2.0V$. The sample rate of the ADCs is determined by the internal clocks and the two clock dividers. 10kHz, 40kHz and 5MHz are the three internal clock frequencies. The first clock divider can divide by 1, 4, 32 and 64. The second clock divider can divide by any number between 1 and 8. Using these dividers and internal clocks there is a lot of choice for a suitable ADC sample frequency.

5.2.2. Basic schematic

In Figure 5.2 a basic schematic of the internal structure of the PPG sensor is shown. It consists of 3 LEDs, LED drivers, photosensitive devices and amplifiers.

The PPG sensor needs to radiate three wavelengths of light into the tissue of the patient to perform measurements: blue, red and infra-red (IR). LEDs are most suited to radiate light as they are small and efficient compared to other light sources. More elaborate design choices for the LEDs are given in section 5.2.3. The MCU is not able to power the LEDs as it can only deliver $1mA$ of current using the GPIO pins, while the LEDs use more than ten times as much to produce enough light. The LEDs will be powered using LED drivers, these can connect the LEDs to the battery which is able to deliver the necessary current based on the state (high-/low) of the GPIO pins. The internal architecture and component choices for the LED drivers are elaborated in more detail in section 5.2.4.

The light that is transmitted into the skin of the patient is mostly attenuated, only a small fraction is reflected back. Two photo sensitive device will produce a small analog output signal with a magnitude proportional to the light intensity of the reflected light. Two devices are needed as the devices sensitive to blue light are not as sensitive to IR and red light and vice versa. More details regarding the photo sensitive device can be found in section 5.2.6. The small output signal is not suitable as an input to the ADC, therefor it needs to be amplified. The amplification ensures for a signal that is more robust against errors that might occur in the ADC. The amplifier should have a high signal to noise ratio to preserve measurement accuracy, In depth analyses and design choices for the amplification step can be obtained in section 5.2.7.

The sensor will operate on two different voltages as it will enable for a better efficiency, this will be explained in more detail in section 5.2.4.

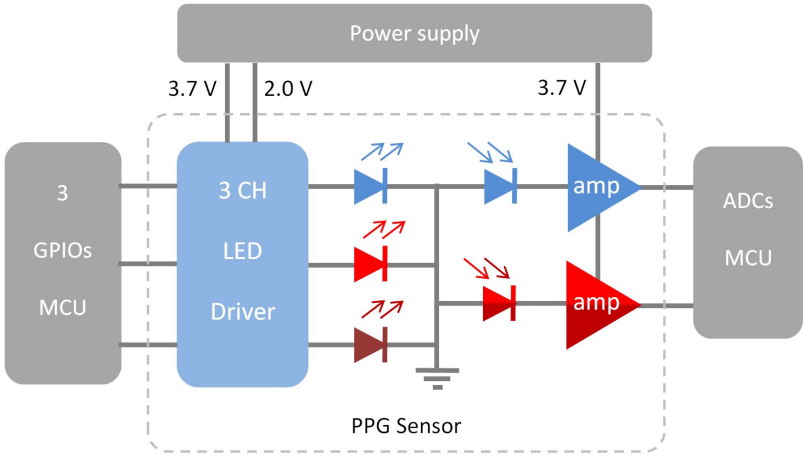

Figure 5.2: Basic schematic of photoplethysmography sensor

5.2.3. LEDs

As small (order of magnitude in millimeters) and efficient (approx. 20%) light sources go LEDs are considered to be the best. The PPG sensor has to remain compact and low power, therefor it will use SMD LEDs for the light source. In this section suitable LEDs are chosen for the PPG sensor. Furthermore, the usefulness of the radiated power is estimated based on the desired light wavelength and angles of radiation. The current needed to power the LEDs will be determined based on the amount of useful radiated power needed for measurements. Finally, LTspice models of the LEDs will be made, these will be used in section 5.2.4 for simulating the effectiveness of the LED drivers. As a reference for determining LED specifications other PPG sensors were used as reference as these are tested and have been proven to work. One of these is the SFH7050 by Osram Opto Semiconductors [31].

Wavelength

As mentioned in section 5.1 the wavelengths 470, 645 and 940 nm of light are needed to measure heart rate, oxygen saturation and bilirubin levels. These are respectively blue, red and infra-red. The LEDs should emit most of the power around these wavelengths, this means a narrow spectral emission peak. From the datasheet of the SFH7050 by Osram Opto Semiconductors [31], mentioned at the start of the section, it can be concluded that the spectral bandwidth with 50% of the maximum intensity should be around 20 nm for the blue and red LED and 40nm for the IR LED for accurate measurements.

Angle of radiation

Another property of LEDs is the majority of power is radiated at zero degrees to the normal of the light emitting surface. As the angle increases less power is radiated. The angle at which only half of the peak radiation intensity is present is called the half angle given in degrees. The LEDs inside available oxygen saturation sensors have a half angle of 60 degrees. With a half angle of 60 degrees the PPG sensor is able to make accurate measurements [31].

Suitable LEDs

The LEDs of Ushio Opto Semiconductors have been selected for the PPG sensor, these fulfill the wavelength and angle of radiation requirements mentioned in the previous two paragraphs. The SMT470, SMT645 and SMT940D are respectively the blue (470 nm), red (645 nm) and IR (940 nm) LEDs used.

To keep the power consumption low, the current use of the LEDs should not be higher than 50mA. At 40mA forward current the LEDs produce 42.32 mW (blue), 23.65 mW (red) and 24.00 mW (IR) of total radiated power. The LEDs in the SFH7050 by Osram produce approximately 4.9 mW (green), 12.8 mW (red) 10.6

mW (IR) at 40mA forward current according to the datasheet. The LEDs by Ushio have a higher light production and are thus well suited for the low power requirements of the PPG sensor.

Useful radiated power
Not all radiated power can be considered useful radiated power for two reasons. Firstly, due to the large angle of light dispersion some light will never reach the photo sensitive element as it is radiated away in opposite direction of the photo sensitive element. It is however, impossible to say without elaborate testing with the used LEDs to predict at which angles the light can be considered not useful. This is mainly due to the close proximity of the sensor to the skin and the high diffusion rate of the skin. It can be said that most radiated power traveling in opposite direction to the light sensitive element will not reach the light sensitive element [28].

Placing the LEDs at an angle could potentially increase the amount of effective light reaching the sensor, however this needs to be experimentally tested and cannot be proven at this time. An assumption based on the high diffusion rate of the skin was made about the useful radiation angles. To calculate the useful radiation power an angle between -40 and 40 degrees was taken as an indication for the loss of useful power.

Secondly some of the radiated power has an undesired wavelength, deviating more than 10 nm for the blue and red LED and 20nm for the IR LED from the dominant wavelength. This radiated power will not be considered useful for the purpose of the PPG sensor.

The LEDs were modelled in Matlab, see appendix A.1, to understand the influence of angle and wavelength on the useful output power. Taking into account the above assumptions only around 40% of the radiated power can be considered useful at a forward current of 40mA for the three different LEDs.

Forward current
Using the above previously mentioned Matlab script the forward current can be determined to produce a particular useful power output for all three LEDs. When more power is radiated into the skin more light will reach the photo sensitive device. When more power reaches the photo sensitive device a larger electrical signal will be produced, which will be less susceptible to noise when amplified. Therefor, the radiated power is maximized while staying within the energy budget. As the IR and red light will be received by the same photo sensitive device the radiated power at the photo sensitive device needs to be of similar magnitude for red and IR light. The absorption of IR and red light may be different and thus the radiated power levels of red and IR light into the skin need to compensate for this.

To achieve the above, the effects of the absorption of melanin for the different wavelengths should be known to compensate for this. As melanin has the highest absorption coefficient of commonly found substances in human skin [4], taking melanin into account gives a good indication. The absorption coefficient is around five times higher for blue (470 nm) than red (645 nm) light and around 10 times higher for blue (470 nm) than IR (940 nm) [10]. The blue LED must radiate a greater amount of power than red and IR to obtain the same radiation intensity at the photo sensitive element. This is extra reason to try to maximize the output power of the blue LED. Furthermore, the output power of the red LED should be twice as large as that of the IR LED.

With 50 mA being the maximum forward current for the blue LED at 25 °C, 45 mA will be considered as the maximum allowed to provide a margin to prevent failure. At 45 mA the useful radiated output power is 17.54 mW of the 46,23 mW total radiated power. The red LED also has a maximum forward current of 50 mA and at 45 mA radiates 11.95 mW useful power of the 26,52 mW total radiated power. The IR LED needs to produce half as much power as the red LED. At 26 mA forward current the IR LED produces 6.06 mW of useful radiated power of the 13.26 mW total radiated power. This is approximately half of the radiated power produced by the red LED.

The useful radiation powers were calculated using an angle between -40°and 40°and a deviating from the dominant wavelength of no more than 10 nm for the blue and red LED and 20nm for the IR LED.

LTspice LED model
In section 5.2.4 simulations will be made in LTspice to design and test LED drivers to deliver the forward currents mentioned in the previous section. To make accurate simulations LTspice models of the LEDs need to be made based on the datasheets. The LTspice model for a LED have 5 parameters: saturation current (Is), emmission coefficient (N), ohmic resistance (Rs), junction capacitance (Cjo) and saturation current temperature exponential (Xti). These parameters are however not given or directly related to values given in the datasheets. To obtain the values for the parameters the Shokley diode equation and the graphs from the datasheet relating forward voltage with forward current and ambient temperature need to be used to emulate the behaviour of the LEDs in a LTspice model.

Table 5.2 shows the parameters and values for each LED for the LTspice model. The method for determining and testing these can be found in appendix A.2. These values have been used to create diodes in the LTspice library for future use.

Table 5.2: The parameters of the LTspice models and their values for the three different LEDs

Parameter	**SMT470**	**SMT645**	**SMT940D**
Saturation current (Is) (in A)	2.45E-19	9.25E-15	1.80E-19
Emmission coefficient (N)	2.7	2.8	1.3
Ohmic resistance (Rs) (in Ω)	8.8	12.3	0.8
Junction capacitance (Cjo) (in pF)	50	50	50
Saturation current temperature exponential (Xti)	90	90	20

5.2.4. LEDs Driver
As described in section 5.2.1 the GPIO pins of the microcontroller cannot supply high enough currents to drive the LEDs. Therefor, a LED driver is designed, which uses the GPIO to connect and disconnect the LEDs with a battery for power. There are two frequently used designs, the first uses an bipolar junction transistor (BJT) and the other a MOSFET, which act as a switch controlled by a control signal. In this case the control signal is the output of the GPIO pin of the microcontroller.

The BJT is a current amplifier, the current leaving the emitter of the transistor is equal to the current going into the base magnified by a component specific factor. The current leaving the emitter of a MOSFET is dependent upon the voltage at the gate of the MOSFET. As BJTs are current driven devices they require a small but constant current supplied to the gate for current to flow through the collector. This is not the case for the MOSFET as it is voltage driven. Furthermore, the collector current from the BJT is more influenced by temperature swings than MOSFETs.

BJTs are used more often to drive LEDs. However as MOSFETs are generally more efficient than BJTs, MOSFETs are used more often in battery supplied loads. Figure 5.3 shows how the MOSFETs are used to power and control the LEDs. Appendix A.3 describes in greater detail how the MOSFET based LED driver is designed and simulated. It will also provide the results of the simulations in greater detail.

The RUM001L02 MOSFET by Rohm Semiconductors will be used for the LED driver circuit as it is designed to drive low currents (max 100mA) using a low gate threshold voltage of 1V. Furthermore, it has a relative low static drain-source on-state resistance of a couple of Ω's, depending on the V_{GS} and I_D, compared to the resistors used to limit the current through the LEDs. Finally a built-in gate-source protection diode is used to promote reliability of the components.

The blue and red LEDs require a larger forward voltage to turn on and will be powered by a 3.7V power supply. The IR LED requires lower voltages and will be powered by the 2.0V secondary power supply also

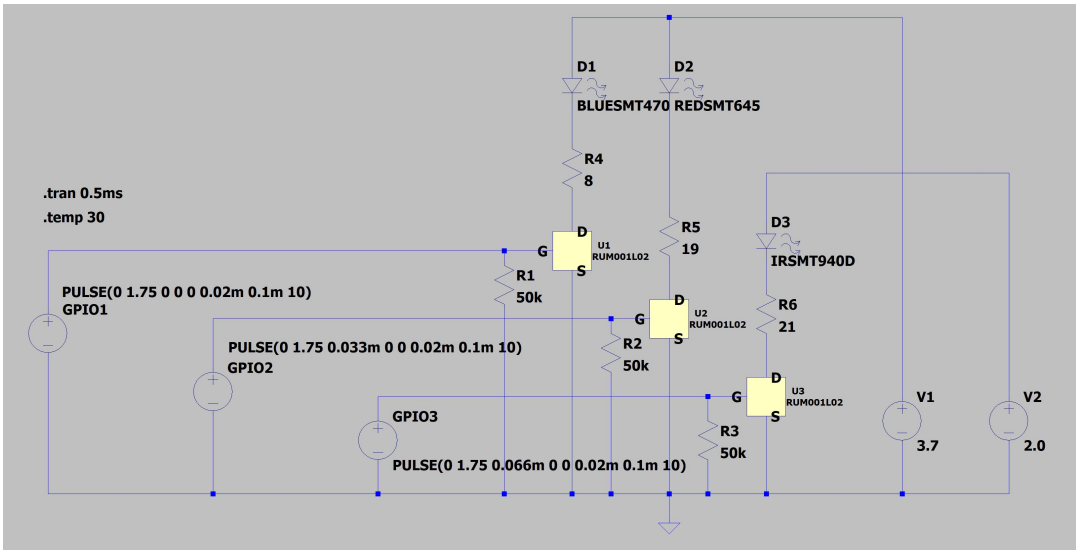

Figure 5.3: Schematic of LED drivers with the three different LEDs, three GPIO pins and the two different power supplies.

used for the temperature sensor, acceleration sensor, microprocessor and BLE module. Being powered also decreases power consumption in resistors in the LED driver circuit.

The simulations further also show the temperature influence on the current through the LEDs, see figure A.10. At 30 °C the LED drivers deliver 45 mA to the blue and red LEDs and 26 mA to the IR LED. The current through the IR LED is 0.2 mA less at 20 °C and 0.2 mA more at 40 °C. The current through the blue and red LEDs is around 1 mA less at 20 °C and around 1 mA more at 40 °C. The changes in current should not influence the measurements greatly.

Regarding power consumption, the LEDs use 142 mW, 120 mW and 35 mW of for respectively blue, red and IR. Efficiency wise, the power delivered to the blue LED is 85.5% of the total power delivered to the Driver. The red LED receives 71.9% of the total power delivered to the driver and the IR LED receives 67.3% of the power. The power not delivered to the LEDs ends up in the resistors that limit the currents through the LEDs and in the MOSFETs, see table A.1 in the appendix the efficiencies are rather poor, especially for the red and IR LEDs, as the supply voltages are not completely ideal to drive the LEDs without using current limiting resistors.

The total energy usages per LED for a measurement of 5 seconds are 166mJ for blue, 167mJ for red and 52mJ for IR. When a measurement is performed once per hour the total power used by the LEDs per day is 9.24J.

5.2.5. Control signals LED drivers

The microcontroller GPIO outputs are used to supply the required voltage to the gate of the MOSFETs to control the state of the MOSFETs. The LEDs need to be turned on one by one to ensure two LEDs are never on simultaneously. Figure 5.4 shows the wave forms of the three GPIO signals. In 100us all three LEDs have been on once for 20us, resulting in a frequency of 10kHz. Only one LED can be on at the same time as otherwise multiple wavelengths of light will hit the same photo sensitive element, leading to the inability to distinguish between the intensity levels of two different light sources. Furthermore, due to current restrictions of 50 mA of the battery only one LED can be powered at a time. The LEDs will turn on and off with a frequency of 10kHz, with only 10 us between when one type of LED turn off and another turns on. This will make it seem as if all the LEDs are on simultaneously, making comparisons between light intensities possible for the three different LEDs. The measuring duration will be five seconds as this will ensure multiple blood pulses have occurred during the measurement process to ensure accurate measurements.

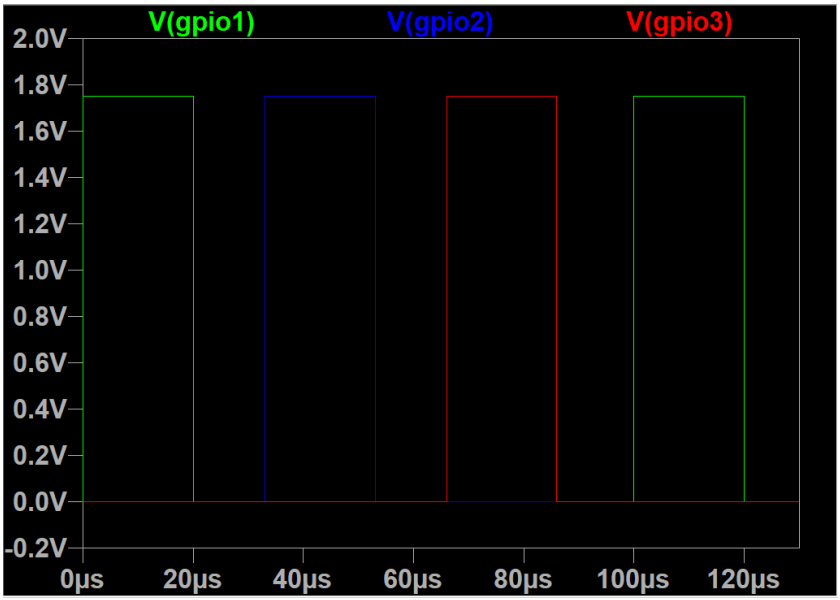

Figure 5.4: Microcontroller GPIO output signals used to control the state of the MOSFETs, which turn on and off the LEDs.

5.2.6. Photo diode

In order to measure the reflected light of the LEDs, photodiodes are used. A photodiode is a semiconductor device which turns light energy into current. In [29] it is stated that the skin will reflect around 0.01% of the radiated power from the LEDs. Therefore, the photodiodes should have a high sensitivity, low noise and a large surface area in order to capture as much light power as possible. In order to detect the red and infrared light for the heart rate and oxygen saturation measurement, a photodiode is chosen which is particularly sensitive for the red and infrared wavelengths. Another photodiode is chosen for the bilirubin sensor. Since bilirubin has a relatively high absorption coefficient in the blue light spectrum, a photodiode which is especially sensitive in the blue light spectrum is chosen.

There are several types of photodiodes available: the PN photodiode, PIN photodiode, the avalanche photodiode and the schottky photodiode.

The PN diode was the first kind of photodiode to be developed. However, nowadays its performance is not as advanced as the more modern types. The depletion zone is were the photo detection occurs and since this zone is relatively small for the PN diode its sensitivity is also smaller than other types of photodiodes.

The PIN photodiode is another version of the PN photodiode. The main difference is that the PIN photodiode has an intrinsic layer between the P and N region. This causes a wider depletion region which results in a larger sensitivity.

The avalanche photodiode is in structure similar to PN and PIN photodiodes. However, opposed to the PN and PIN photodiodes, an avalanche photodiode operates with a large reverse bias voltage. Due to this large bias voltage a strong electric field is generated which accelerates the electrons. When the bias voltage is high enough these electrons will be accelerated enough to create ionization in the lattice. Therefore, more free charge carriers will be created and this will lead to even more ionization. This results in a large current. An avalanche diode is therefore highly sensitive but not linear in its output due to this avalanche process.

The schottky photodiode has the same working principle as the schottky diode. As opposed to the earlier discussed photodiodes the schottky photodiode utilizes a metal-semiconductor junction instead of a p-n junction. The operation and structure is similar to the PIN photodiode except for the lack of p-type region. However, due to the reflection and absorption in the metal layer this type op photodiode tends to be less efficient.

For the designed circuit PIN photodiodes are chosen due to their high sensitivity and efficiency. The avalanche photodiode is not chosen since the circuit will not operate on a high enough voltage.

5.2.7. Amplifier

Since the reflected light which will be collected by the photodiode will be of very low power, the photodiode will generate a small current. In order to be useful the incoming signal needs to be amplified. This is achieved by using a transimpedance amplifier. This type of amplifier converts the signal current into a voltage. In the designed circuit the photodiode will operate in photovoltaic mode. This means there is no bias voltage across the diode which means the dark current of the photodiode is at a minimum.

The first design step for the transimpedance amplifier is calculation the value for the feedback resistor. This value depends on the diode output current and the supply voltage, see Equation 5.1.

$$R_f = \frac{V_{cc}}{I_{ph}} \tag{5.1}$$

However, the maximum voltage the micro controller can receive is 2V. Therefore, assuming a maximal input current signal of 15.6μA, the value for the feedback resistor will be 128$k\Omega$.

In order to stabilize the circuit a feedback capacitor is added. This capacitors value is dependent on the input capacitance of the amplifier, the feedback resistor and the desired bandwidth, see Equation 5.2.

$$C_f = \sqrt{\frac{C_{in}}{2\pi R f_t}} \tag{5.2}$$

C_{in} in Equation 5.2 is the sum of the junction capacitance of the photodiode (C_j), the differential input capacitance of the amplifier (C_d) and the common-mode input capacitance (C_m). In the designed circuit the input capacitance would result in a value of 78 pF. The measurements will be performed with a sample frequency of 10 kHz which means that according to Equation 5.2 the value of the feedback resistor will be 98 pF.

In order to keep the amplifier from being saturated when the input current is zero, a reference voltage of 0.1V is applied to the positive terminal of the amplifier, see Equation 5.3.

$$R7 = \frac{V_{cc} - V_{ref}}{V_{ref}} \cdot R8 \tag{5.3}$$

Since the supply voltage is 3.7V this will result in the following resistor ratio: $R7 = 36 \cdot R8$. In the designed circuit for $R8 = 10k\Omega$ which means $R7 = 360k\Omega$.

The designed circuit used in the simulation program LTspice is shown in Figure 5.5. The photodiode is modelled as a current source with a capacitor and a resistor in parallel. These components represent the diode current, the junction capacitance and the shunt resistance of the photodiode. During the simulations, the calculated value for the feedback capacitor did not result in a clean output signal. Therefore, a lower value was used, determined by making further simulations.

The simulation is shown in Figure 5.6.

As can be seen from the simulation the designed sensor has a linear output voltage as a function of the input signal current.

The same procedure is performed for the bilirubin circuit. The resulting design is similar as is shown in 5.5. The only difference is that the values for the equivalent circuit of the photodiode are slightly different, see Figure A.11. In Figure A.12 one period of a bilirubin measurement is shown. In the figure the output voltage is shown for three different temperatures: 20°C, 30 °C and 40 °C. As can be seen from the figure the temperature does not have a significant influence in the output signal.

5.2.8. Placing of LEDs and photo collector

In order to obtain the optimal measurement result the correct placing of the LEDs and the photodiodes is very important. In order to save space only the LEDs and the photodiodes are placed at the skin side of the PCB. The amplifiers and drivers are place on the other side. In [13] the optimal distance between the LED and

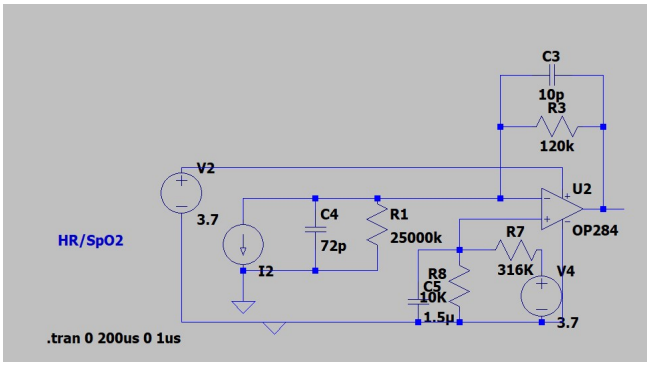

Figure 5.5: Design Heart rate and oxygen saturation sensor

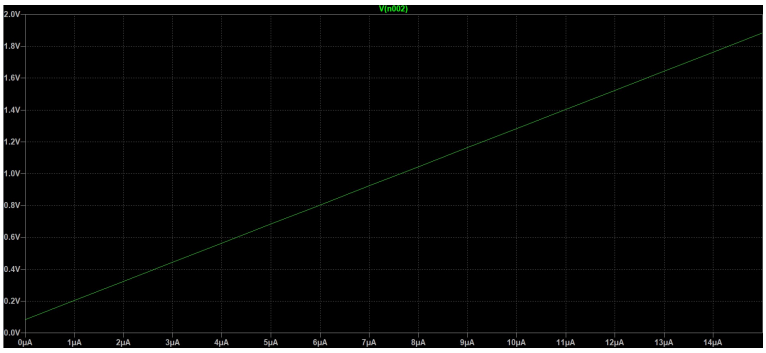

Figure 5.6: Design Heart rate and oxygen saturation sensor simulation

the photodiodes is determined. It is shown that a distance between 3-6 mm yielded the best results. In [29] it is concluded that the distance at which the LED and the photodiodes need to be placed depends on the depth at which the pulsating blood vessels are located. The deeper the blood vessels are located the larger the distance needs to be. Since the sensor patch will be attached to the chest where the pulsating blood vessel lay relatively deep in under the skin as opposed to for example a finger or an earlobe, a distance of 6 mm is chosen.

5.3. Conclusion

The designed PPG sensor is theoretically able to perform measurements of heart rate, oxygen saturation and bilirubin while being placed on the chest.

The LEDs use 9.24J of energy per day when a measurements last for 5 seconds and are performed once per hour. The peak power consumption of the amplifiers is 3.68 mW per amplifier. Therefore, when measurements are performed once per hour and take 5s per measurement the total energy consumption per day by the amplifiers is 0.88J. The total energy consumption of the PPG sensor is 10.12J per day. The design requirement was that 18J per day was allocated for use by the PPG sensor, therefor the PPG sensor fulfills the energy design requirements.

Using Table B, an estimate of the surface area covered by the PPG sensor can be made. The photodiodes and LEDs require the most space as the LEDs must be placed at around 0.6 cm from the photodiodes. The bottom side of the 2 x 3 cm will mostly have to be used for this. The top side will contain the LED drivers and amplifiers, these will require no more than an area of 2 x 1.5 cm. Leaving enough room for the placement of the temperature and acceleration sensors.

Using Table B again an estimate can be made of the component costs of the PPG sensor. Adding up all the prices of the individual components results in a total price of €22 for the PPG sensor. This is less than the 30 that was set as a maximum price in the requirements and thus the price requirement has been met.

The sensor is powered by two voltage supplies, 2V and 3.7V, these are both lower than the voltage requirement of 5V, Furthermore, the total current draw from the PPG sensor is less than 50 mA as was required.

As can be seen in Section 5.2.6, the skin reflects around 0.01% of the radiated power by the LEDs. Since the 46mW is radiated by the blue LED, 26mW by the red LED and 13mW infrared LED, the received power by the photodiodes will be in the order of $1\mu W$. This is thereafter transformed into a current by the photodiode which is finally amplified to a maximum voltage by the amplifiers.

6

Overal design

This chapter discusses what the prototype should look and perform like. First, the physical characteristics will be discussed. Then a section will be devoted to how the system should be used.

6.1. Physical characteristics prototype

Figure 6.1, 6.2 and 6.3 show the top view, side view and bottom view respectively of the design of the sensor patch. The total size should be 3x7cm since this was recommended by Dr. Dudink [1]. The orange parts are flexible wires that interconnect the different parts. These flexible wires allow the prototype to be closer to the skin of the patient. Since the device needs to be reusable, it should be possible to clean the device. Therefore the device should be water- and alcohol proof. To this end, a silicon layer will be applied over the entire device. This will result in a flexible reusable device.
Additionally there will be 2 contact points on the silicon casing through which the battery can be charged.

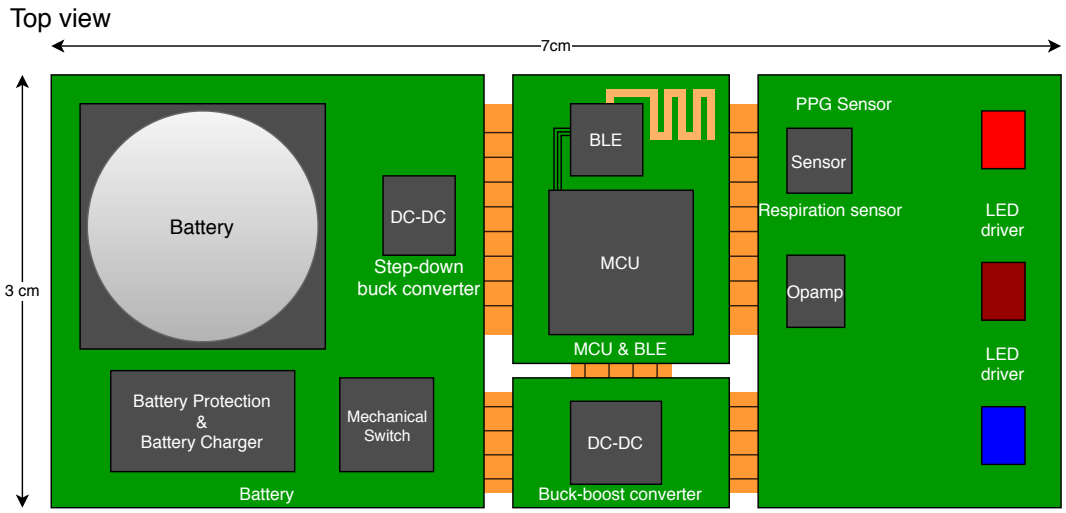

Figure 6.1: Top view of physical prototype

6.2. Results of final design

The photoplethysmography (PPG) sensor measuring heart rate, oxygen saturation and bilirubin levels has been designed to make accurate measurements theoretically possible. This was based on the following: sensor properties form papers describing similar PPG sensors, LED radiated power, attenuation and diffusion factors of the skin, photo-diode sensitivity and output currents and noise due to the amplification of the photo-diode output. However as no physical prototype has been made, no measurements could be per-

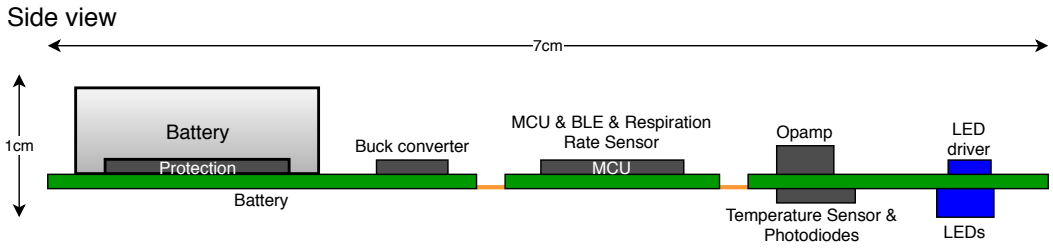

Figure 6.2: Side view of physical prototype

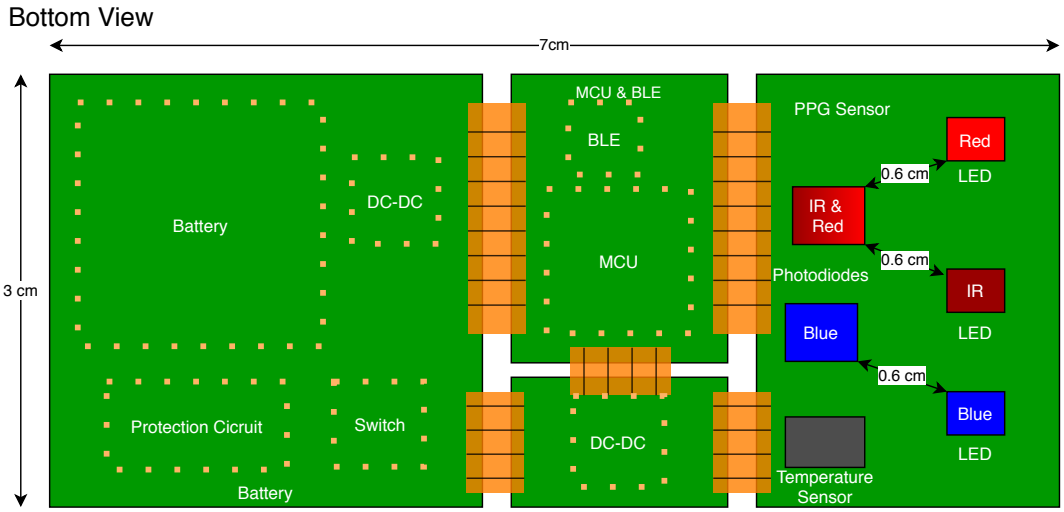

Figure 6.3: Bottom view of physical prototype

formed to proof the accuracy and measurement capabilities when performing measurements on patients.

The temperature sensor (Si7051) is able to perform accurate measurements within 0.1 degrees Celsius deviation between measured skin temperature and actual skin temperature. There is a correlation between skin temperature at the chest and internal core temperature [26]. Heart rate and chest movements are used for the correlation model and enable noninvasive methods to replace invasive methods to monitor patient core temperature.

The acceleration sensor (IIS2DLPC) produces 3 dimensional acceleration data with a acceleration resolution of 0.224mg. Using algorithms that remove large body movement components a method for estimating respiration rate can be used to measure respiration rate [12]. Studies have shown accurate respiration rates can be measured when using a 3D acceleration sensor with a sensitivity of 0.2mg and the appropriate signal processing techniques [24].
The total system consumes an estimated 52J in 3 days when it is attached to a newborn while measuring once every hour. This energy consumption is the sum of deep sleep, wake up, measurement, processing and transmission stages of every device separately. A visualisation can be seen in Figure 6.4. The sensor patch can last an estimated 3 weeks on one battery cycle.
The system is able to communicate its measurements wirelessly to a Bluetooth receiving device. This can either be a mobile phone, or some sort of base station which should be developed further.

6.3. Conceptual use case

6.3.1. Data access

In terms of usability, there are a few factors which should be considered. Firstly, this system will measure and transmit sensitive medical data. Only doctors or nurses, who would otherwise work in the maternity ward of the hospital shall be allowed insight into this information. Parents should not be able to view the

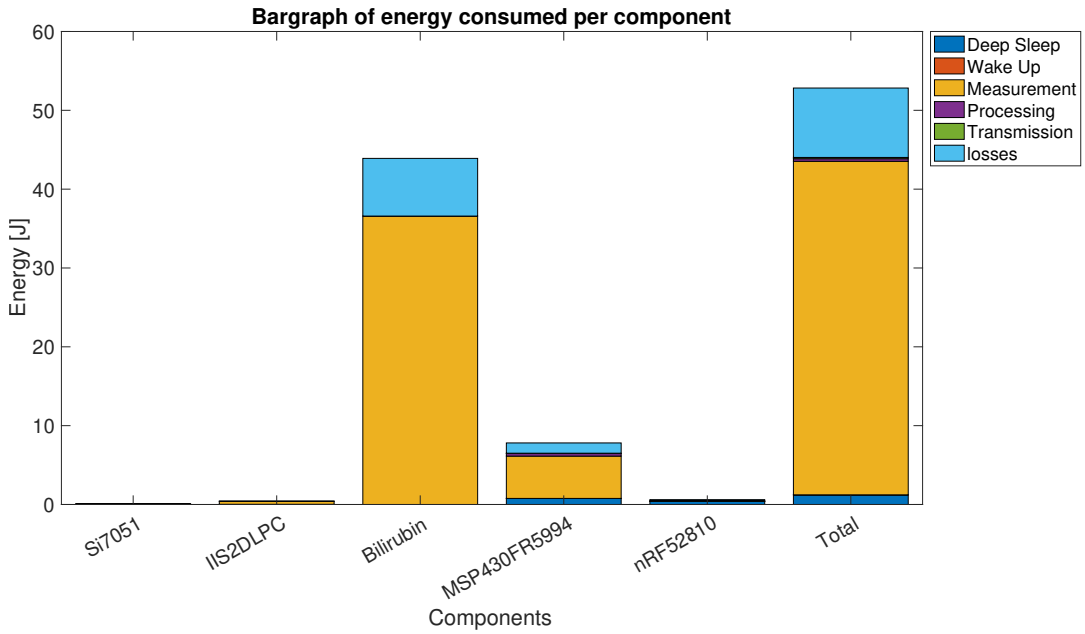

Figure 6.4: Energy usage per component divided per stage in the full system simulation.

measurements from the patch since they are not trained to interpret this medical information and the risk of unnecessary panic would be great. The purpose of this project is to replace maternity care and offer the possibility of medical monitoring from home, but this monitoring shall still only be interpreted by medical professionals.

6.3.2. Application of patch on skin

The first time the sensor patch is attached will be in maternity care. This will be done by a nurse. This way it is ensured that the sensor patch will be applied properly the first time, before the baby goes home. As described in further detail in Section 6.6, the patch will have an indicator which indicates if it is applied properly. Because of this indicator, parents at home could also reapply the patch properly in case this is needed.

6.3.3. Charging

The charging of the sensor patch will be done by trained individuals, to avoid accidental overcharging or damage to the system. This charging shall be done at the same location as the sterilisation of the devices as described in Section 6.4.

6.4. Sterilisation methods

The sensor patch can be categorised as a Semi-critical instrumentation, which means that it needs to be cleaned and disinfected [11]. Sterilisation often happens with alcohol and/or steam. The device will have a silicon layer around it as mentioned earlier. For this application, alcohol can be used to sterilise because silicone has good chemical resistance for alcohol [22].

6.5. Conclusion

As can be seen in Figure 6.1 the final design of the sensor patch does not exceeds the required dimensions mentioned in 2. Furthermore, the designed sensor patch is able to measure the heart rate, temperature, oxygen saturation, respiration and bilirubin. The battery is able to supply enough power to perform measurements every 2 hours for 3 days. Moreover, the sensor patch is able to communicate wirelessly with an external device in order to send the measured data to a hospital where a doctor can access this data.

6.6. Future work

Some aspects of the design have not yet been addressed in this paper. In order to implement the sensor patch successfully, some aspects still need to be researched. They will be discussed in this chapter section.

6.6.1. Patch contact indicator

In order to receive accurate measurements from the sensor patch, it needs to be attached properly. Otherwise, the sensors might might be too far away from the skin for accurate measurements. For this purpose, further work needs to be done into the development of some sort of indicator which will inform the user whether the patch is applied properly to the skin, so that the user can expect correct measurements.

6.6.2. PCB

A concept for the construction of a PCB and component placement has been made, however a design and testing procedure must take place in the future to realise a PCB with the correct placement and operation of components. The PCB design has to take into account aspects of comfort and durability to fulfil design requirements. Flexible PCBs or flexible cables need to be explored to see if the sensor patch can be somewhat flexible to make it fit better to the skin of the patient.

6.6.3. PCB housing

In order to protect the sensor patch from external influences, the patch needs a casing. This case must be completely closed and non transparent in order to block the ambient light which could influence the PPG sensors. However, this casing should not interfere with the Bluetooth communication. Furthermore, the casing should protect the electronics of the sensor patch from moisture like sweat. In order to increase user comfort the casing should be flexible. Also, charging points will need to be integrated in the PCB housing.

6.6.4. Method of attachment

No testing has been performed on how to apply the sensor patch to the patient. Some solutions have been conceived such as: using an adhesive material or tape to secure the sensor patch. These methods need to be explored and tested in the future to determine their capabilities of attaching the sensor patch for a period of three days. Water resistance can be a useful property for the method of attachment as this would enable the patient to take a bath while wearing the sensor patch and would prevent the patch from losing grip if the patient sweats.

6.6.5. Clinical trials

In order to calibrate the designed sensors, clinical trials on patients should be performed. The trials can be used to remove systematic errors in the measurements. Furthermore trials would also verify the performance of the sensors, for example the accuracy and repeat-ability of measurements. The trials will reveal potential issues in the design and may lead to the need of design alterations.

7

Conclusion and future work

7.1. Conclusion

As can be read in previous chapters, the required sensors, which are stated in 2, are chosen or designed. The total price of these sensor would be approximately 28 euros (see Appendix B which is less than the required 40 euros. The dimensions of the chosen and designed sensors are all small enough to fit on the designated area on the sensor patch. Furthermore, the total energy consumption is 10.2J per day which is well under the required 20J per day. In the design of the sensor the communication with the microcontroller is taken into account.

7.2. Future work

The sensors have been chosen or designed based on theoretical models, simulations and other articles using similar techniques. There have been no trials performed on patients to prove the sensor system works. Several steps regarding the different sensors need to be taken to enable the testing of a prototype of the complete sensor system:

Temperature sensor

1. Design and implement algorithms to correlate chest skin temperature to internal core temperature
2. Calibrate the sensors using a number of test subjects
3. Perform temperature tests on a large group of babies to determine the accuracy of the temperature sensor and the algorithms surrounding it.
4. Determine the effects of heat production by surrounding components in the 'Sensor Patch' (i.e., microprocessor, LEDs) on the accuracy of the sensor

Respiration rate sensor

1. Design and implement algorithms to convert raw sensor data from 3-axis acceleration sensor into a value for the respiration rate.
2. Calibrate the sensors using a number of test subjects
3. Perform respiration rate tests on a large group of babies to determine the accuracy of the sensor and the algorithms surrounding it.
4. explore the use of combining sensors to improve the accuracy of estimating respiration rate (i.e., gyroscopes, magnetometers).

PPG

1. Measure accurately the amount of reflected light received by a photodiode for the three different wavelengths at different separation distances between LED and photodiode.

2. Determine based on the previous point if the radiated power by the LEDs is sufficient for the given photodiodes to make accurate measurements of the pulsatile volume of blood.
3. Determine the proper ratios of radiated power between the different wavelengths of light.
4. Determine based on the above if the design of the amplifier stage is still appropriate and perform physical test to prove this.
5. Design and implement algorithms to accurately estimate heart rate, oxygen saturation and bilirubin levels based on the output data from the photodiodes.
6. Calibrate the sensors using a number of test subjects.
7. Perform tests on a large group of babies to determine the accuracy of the sensor and the algorithms.
8. Study the effect of a housing designed to protect the sensors against water on the accuracy of the sensor.

List of Figures

List of Tables

A

PPG sensor design

A.1. MATLAB scripts and plots calculating useful output power LEDs

A.1.1. Blue LED SMT470

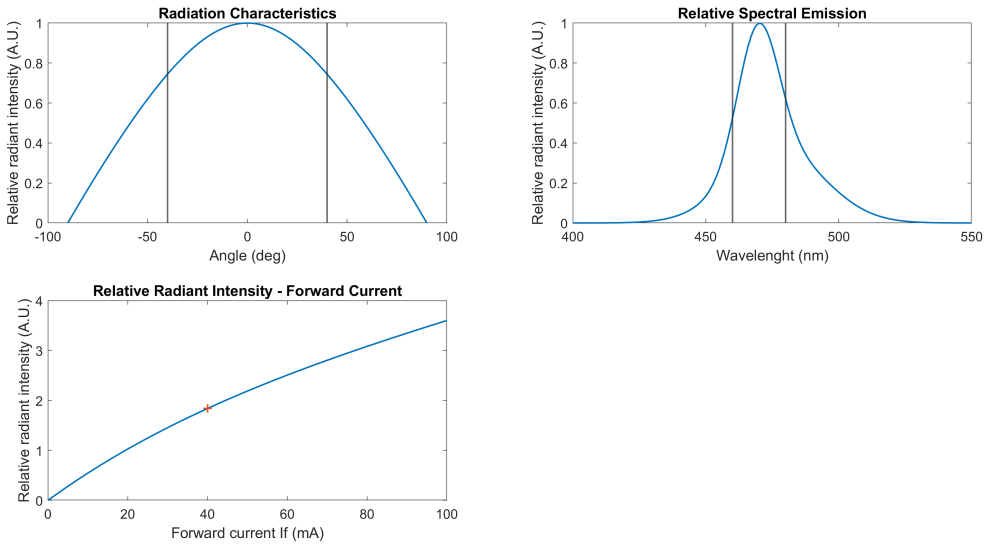

Figure A.1: Plots created by matlab script (listing A.1) illustrating how the useful radiated power is calculated for the SMT470 blue LED. For the top two plots the area under the curve and between the vertical lines is taken to determine the fraction of useful power

Listing A.1: MATLAB script calculating the useful output power of the blue SMT470 LED

```
close all
clear all

% Matlab script can  be used to calculate the amount of useful power radiated by the blue LED
    in the form of light. This is dependent upon the forward current through the LED, the max
    and min radiation angle and the min and max wavelength that belong to the useful part of
    the radiated output light.

%% Specifications BLUE LED

Power_If_20 = 23;   %Total power output at forard current If = 20mA (in mW)

%% Variables influencing total useful output power
```

```
angle_min = -40;
angle_max = 40;
wavelength_min = 460;
wavelength_max = 480;
If_LED = 40;
%If_LED = 34;

%% normalized output power angle

% Equation and values for a,b,c determined using the datasheets and the curve fitting tool.
a1 = 0.9885;
b1 = 0.01757;
c1 = 1.571;
a2 = 0.01146;
b2 = 0.0653;
c2 = 1.571;

BLUE_angle_fit = -90:0.1:90;
x = BLUE_angle_fit;
BLUE_RRI_angle_fit = a1.*sin(b1.*x+c1) + a2.*sin(b2.*x+c2);

fun = @(x) a1.*sin(b1.*x+c1) + a2.*sin(b2.*x+c2);
xmin = angle_min;
xmax = angle_max;
Useful_output_power = integral(fun,xmin,xmax);
Total_output_power = integral(fun,-90,90);
norm_output_power_angle = Useful_output_power/Total_output_power;     %Fraction of useful power
    based on radiation angle limits

%% normalized output power wavelength

% Equation and values for a,b,c determined using the datasheets and the curve fitting tool.
a1 =  0.6665;
b1 =  469.7;
c1 =  10.76;
a2 =  0.3605;
b2 =  477;
c2 =  24.88;

BLUE_wavelength_fit = 400:1:550;
x = BLUE_wavelength_fit;
BLUE_RRI_wavelength_fit = a1*exp(-((x-b1)./c1).^2) + a2*exp(-((x-b2)./c2).^2);

fun = @(x) a1*exp(-((x-b1)./c1).^2) + a2*exp(-((x-b2)./c2).^2);
xmin = wavelength_min;
xmax = wavelength_max;
Useful_output_power = integral(fun,xmin,xmax);
Total_output_power = integral(fun,350,550);
norm_output_power_wavelength = Useful_output_power/Total_output_power;  %Fraction of useful
    power based on wavelength limits

%% normalized output power forward current

% Equation and values for a,b,c determined using the datasheets and the curve fitting tool.
a = 2.703;
b = 0.004098;
c = -2.706;
d = -0.01745;

BLUE_If_fit = 0:0.1:100;
```

```
x = BLUE_If_fit;
BLUE_RRI_If_fit = a.*exp(b.*x) + c.*exp(d.*x);

norm_output_power_If = a.*exp(b.*If_LED) + c.*exp(d.*If_LED);   %Fraction of output power
    based on forward current through LED.

%% Total output power

Total_useful_output_power = norm_output_power_If * norm_output_power_wavelength *
    norm_output_power_angle * Power_If_20;

%% Plots

% Visualization of the selected values for the variables influencing total useful output power
subplot(2,2,1)
plot(BLUE_angle_fit,BLUE_RRI_angle_fit)
ylim([0 1]);
xline(angle_min);
xline(angle_max);
title('Radiation Characteristics')
xlabel('Angle (deg)')
ylabel('Relative radiant intensity (A.U.)')

subplot(2,2,2)
plot(BLUE_wavelength_fit,BLUE_RRI_wavelength_fit)
xline(wavelength_min);
xline(wavelength_max);
title('Relative Spectral Emission')
xlabel('Wavelenght (nm)')
ylabel('Relative radiant intensity (A.U.)')

subplot(2,2,3)
plot(BLUE_If_fit,BLUE_RRI_If_fit,If_LED,norm_output_power_If,'*')
title('Relative Radiant Intensity - Forward Current')
xlabel('Forward current If (mA)')
ylabel('Relative radiant intensity (A.U.)')
```

A.1.2. Red LED SMT645

Listing A.2: MATLAB script calculating the useful output power of the red SMT645 LED

```
close all
clear all

% Matlab script can  be used to calculate the amount of useful power radiated by the red LED
    in the form of light. This is dependent upon the forward current through the LED, the max
    and min radiation angle and the min and max wavelength that belong to the useful part of
    the radiated output light.

%% Specifications RED LED

Power_If_20 = 11;   %Total power output at forward current If = 20mA (in mW)

%% Variables influencing total useful output power

angle_min = -40;
angle_max = 40;
wavelength_min = 635;
wavelength_max = 655;
If_LED = 40;
```

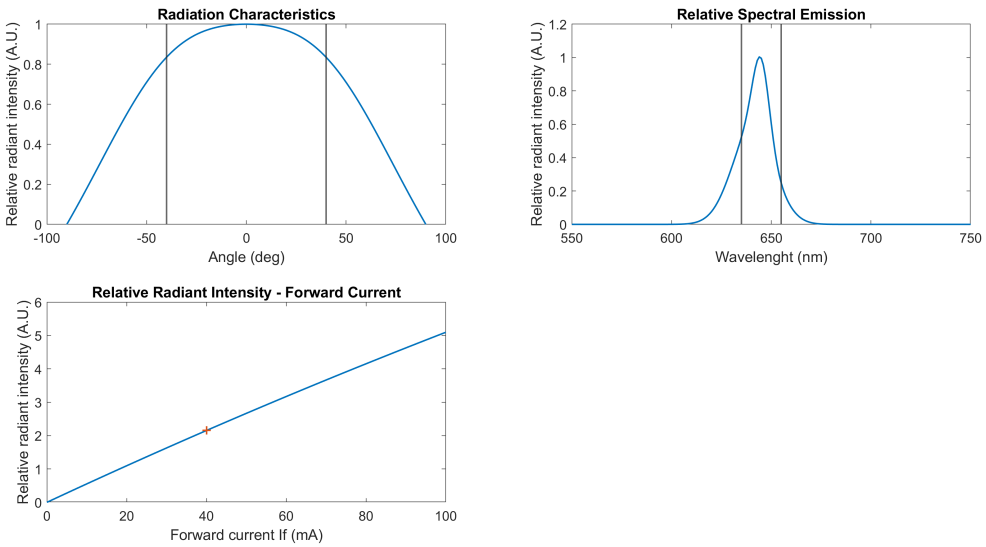

Figure A.2: Plots created by matlab script (listing A.2) illustrating how the useful radiated power is calculated for the SMT645 red LED. For the top two plots the area under the curve and between the vertical lines is taken to determine the fraction of useful power

```
%If_LED = 42;

%% normalized output power angle

% Equation and values for a,b,c determined using the datasheets and the curve fitting tool.
a1 = 1.034;
b1 = 0.01709;
c1 = 1.571;
a2 = 0.03421;
b2 = 0.07174;
c2 = -1.571;

RED_angle_fit = -90:0.1:90;
x = RED_angle_fit;
RED_RRI_angle_fit = a1.*sin(b1.*x+c1) + a2.*sin(b2.*x+c2);  %Fraction of useful power based on
    radiation angle limits

fun = @(x) a1.*sin(b1.*x+c1) + a2.*sin(b2.*x+c2);
xmin = angle_min;
xmax = angle_max;
Useful_output_power = integral(fun,xmin,xmax);
Total_output_power = integral(fun,-90,90);
norm_output_power_angle = Useful_output_power/Total_output_power;

%% normalized output power wavelength

% Equation and values for a,b,c determined using the datasheets and the curve fitting tool.
a1 = 0.4621;
b1 = 644.9;
c1 = 5.846;
a2 = 0.5796;
b2 = 640.8;
c2 = 14.59;

RED_wavelength_fit = 550:1:750;
x = RED_wavelength_fit;
RED_RRI_wavelength_fit = a1.*exp(-((x-b1)./c1).^2) + a2.*exp(-((x-b2)./c2).^2); %Fraction of
```

```
    useful power based on wavelength limits

fun = @(x) a1.*exp(-((x-b1)./c1).^2) + a2.*exp(-((x-b2)./c2).^2);
xmin = wavelength_min;
xmax = wavelength_max;
Useful_output_power = integral(fun,xmin,xmax);
Total_output_power = integral(fun,550,750);
norm_output_power_wavelength = Useful_output_power/Total_output_power;

%% normalized output power forward current

% Equation and values for a,b,c determined using the datasheets and the curve fitting tool.
a = 4.293e+04;
b = -0.000909;
c = -4.293e+04;
d = -0.0009103;

RED_If_fit = 0:0.1:100;
x = RED_If_fit;
RED_RRI_If_fit = a.*exp(b.*x) + c.*exp(d.*x);

norm_output_power_If = a.*exp(b.*If_LED) + c.*exp(d.*If_LED);   %Fraction of output power
    based on forward current through LED

%% Total output power

Total_useful_output_power = norm_output_power_If * norm_output_power_wavelength *
    norm_output_power_angle * Power_If_20;

%% Plots

% Visualization of the selected values for the variables influencing total useful output power
subplot(2,2,1)
plot(RED_angle_fit,RED_RRI_angle_fit)
ylim([0 1]);
xline(angle_min);
xline(angle_max);
title('Radiation Characteristics')
xlabel('Angle (deg)')
ylabel('Relative radiant intensity (A.U.)')

subplot(2,2,2)
plot(RED_wavelength_fit,RED_RRI_wavelength_fit)
xline(wavelength_min);
xline(wavelength_max);
title('Relative Spectral Emission')
xlabel('Wavelenght (nm)')
ylabel('Relative radiant intensity (A.U.)')

subplot(2,2,3)
plot(RED_If_fit,RED_RRI_If_fit,If_LED,norm_output_power_If,'*')
title('Relative Radiant Intensity - Forward Current')
xlabel('Forward current If (mA)')
ylabel('Relative radiant intensity (A.U.)')
```

A.1.3. IR LED SMT940D

Listing A.3: MATLAB script calculating the useful output power of the IR SMT940D LED

```
close all
clear all
```

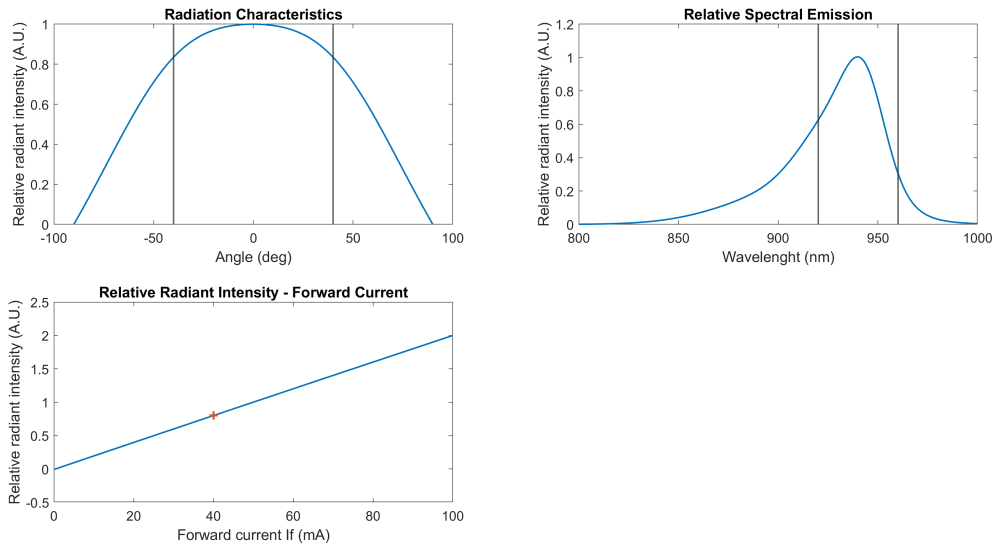

Figure A.3: Plots created by matlab script (listing A.3) illustrating how the useful radiated power is calculated for the SMT940D IR LED. For the top two plots the area under the curve and between the vertical lines is taken to determine the fraction of useful power

```
% Matlab script can  be used to calculate the amount of useful power radiated by the IR LED in
    the form of light. This is dependent upon the forward current through the LED, the max
    and min radiation angle and the min and max wavelength that belong to the useful part of
    the radiated output light.

%% Specifications IR LED

Power_If_50 = 30;    %Total power output at forard current If = 50mA (in mW)

%% Variables influencing total useful output power
angle_min = -40;
angle_max = 40;
wavelength_min = 920;
wavelength_max = 960;
If_LED = 40;
%If_LED = 37.5;

%% Normalized output power angle

% Equation and values for a,b,c determined using the datasheets and the curve fitting tool.
a1 = 1.034;
b1 = 0.01709;
c1 = 1.571;
a2 = 0.03421;
b2 = 0.07174;
c2 = -1.571;

IR_angle_fit = -90:0.1:90;
x = IR_angle_fit;
IR_RRI_angle_fit = a1.*sin(b1.*x+c1) + a2.*sin(b2.*x+c2);

fun = @(x) a1.*sin(b1.*x+c1) + a2.*sin(b2.*x+c2);
xmin = angle_min;
xmax = angle_max;
Useful_output_power = integral(fun,xmin,xmax);
Total_output_power = integral(fun,-90,90);
norm_output_power_angle = Useful_output_power/Total_output_power;    %Fraction of useful power
```

```
    based on radiation angle limits

%% Normalized output power wavelength

% Equation and values for a,b,c determined using the datasheets and the curve fitting tool.
a1 = 0.4657;
b1 = 943.3;
c1 = 14.08;
a2 = 0.4924;
b2 = 931.2;
c2 = 25.24;
a3 = 0.2022;
b3 = 908.5;
c3 = 46.33;

IR_wavelength_fit = 800:1:1000;
x = IR_wavelength_fit;
IR_RRI_wavelength_fit = a1.*exp(-((x-b1)./c1).^2) + a2.*exp(-((x-b2)./c2).^2) + a3.*exp(-((x-
    b3)./c3).^2);

fun = @(x) a1.*exp(-((x-b1)./c1).^2) + a2.*exp(-((x-b2)./c2).^2) + a3.*exp(-((x-b3)./c3).^2);
xmin = wavelength_min;
xmax = wavelength_max;
Useful_output_power = integral(fun,xmin,xmax);
Total_output_power = integral(fun,800,1000);
norm_output_power_wavelength = Useful_output_power/Total_output_power;  %Fraction of useful
    power based on wavelength limits

%% Normalized output power forward current

% Equation and values for a,b,c determined using the datasheets and the curve fitting tool.
a = 6.271;
b = 0.00146;
c = -6.279;
d = -0.001777;

IR_If_fit = 0:0.1:100;
x = IR_If_fit;
IR_RRI_If_fit = a.*exp(b.*x) + c.*exp(d.*x);

norm_output_power_If = a.*exp(b.*If_LED) + c.*exp(d.*If_LED);   %Fraction of output power
    based on forward current through LED

%% Total useful output power

Total_useful_output_power = norm_output_power_If * norm_output_power_wavelength *
    norm_output_power_angle * Power_If_50;

%% Plots

%Visualization of the selected values for the variables influencing total useful output power
subplot(2,2,1)
plot(IR_angle_fit,IR_RRI_angle_fit)
ylim([0 1]);
xline(angle_min);
xline(angle_max);
title('Radiation␣Characteristics')
xlabel('Angle␣(deg)')
ylabel('Relative␣radiant␣intensity␣(A.U.)')

subplot(2,2,2)
```

```
plot(IR_wavelength_fit,IR_RRI_wavelength_fit)
xline(wavelength_min);
xline(wavelength_max);
title('Relative Spectral Emission')
xlabel('Wavelenght (nm)')
ylabel('Relative radiant intensity (A.U.)')

subplot(2,2,3)
plot(IR_If_fit,IR_RRI_If_fit,If_LED,norm_output_power_If,'*')
title('Relative Radiant Intensity - Forward Current')
xlabel('Forward current If (mA)')
ylabel('Relative radiant intensity (A.U.)')
```

A.2. Method for creating LED LTspice models

At the end of section 5.2.3 the parameters and values for a LTspice model were given for three LEDs. In this part of the appendix the methods for finding these values and a measure of the accuracy of the LTspice model to the datasheets is given.

A.2.1. Saturation current and emission coefficient

An ideal diode can be modelled using the Shokley diode equation, this will give the voltage current relationship of an ideal diode. Equation A.1 gives the Shokley diode equation.

$$I = I_S(e^{\frac{V_D}{nV_T}} - 1) \tag{A.1}$$

where:
I is the current through the diode in A
I_S is the saturation current in A
V_D is the voltage across the diode in V
n is the emission coefficient also know as the quality factor
V_T is the thermal voltage

The thermal Voltage is given by equation A.2. For $T = 303K(30°C)$ the thermal voltage is approximately $26.12mV$.

$$V_T = \frac{kT}{q} \tag{A.2}$$

The forward voltage and forward current relationship of the LEDs were plotted in Excel using the figures found in the datasheets. The Shokley diode equation was also plotted in the same Excel plots. The plots were given a logarithmic scale for the y-axis. The I-V curve of the LED should represent an almost linear line at low forward voltages. The Shokley diode equation also gives a linear line when a logarithmic scale is used. The values for I_S and n should be given such values that the Shokley diode line matches the I-V curve of the LED for low forward voltages. The emission coefficient n determines the angle with the x-axis and the saturation current I_S determines the vertical offset of the Shokley diode line. Figures A.4, A.5 and A.6 show how well the Shokley diode equation fits the datasheets in the linear part with a logarithmic y-axis.

Using the values for I_S and n a very basic LTspice for the LEDs can be made. Adding **.model ledtest D (Is='value for Is' N='value for N' Rs=10)** to the diode library of LTspice will enable to determine the other three parameters in LTspice. The ohmic resistance R_S is set to an arbitrary resistance of 10Ω, this will be changed later to fit the model to the datasheet.

A.2.2. Ohmic resistance

In LTspice the LTspice LED model was connected to a voltage source. Performing a simulation using a DC sweep from 0 to 4 V and measuring the current through the LED will result in a I-V curve. This curve needs to be matched to the curve of the datasheet for all forward voltages. This can be done by altering the value of R_S. R_S influences the roll off effect due to ohmic resistance. Increasing R_S increases the roll off effect and will decrease the forward current for the forward voltage in the higher voltage range. A good fit to the datasheet

can be made by choosing the appropriate values for I_S, N and R_S. Figures A.4, A.5 and A.6 show how well the LTspice models fit the datasheets for the SMT470, SMT645 and SMT490D LEDs respectively.

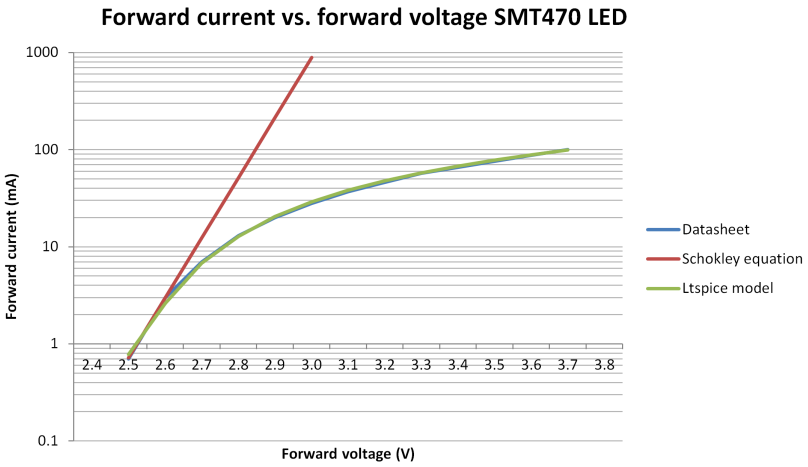

Figure A.4: Excel plot showing the forward current forward voltage relationship of the blue SMT470 LED based on the datasheet, Shokley diode equation and LTspice model.

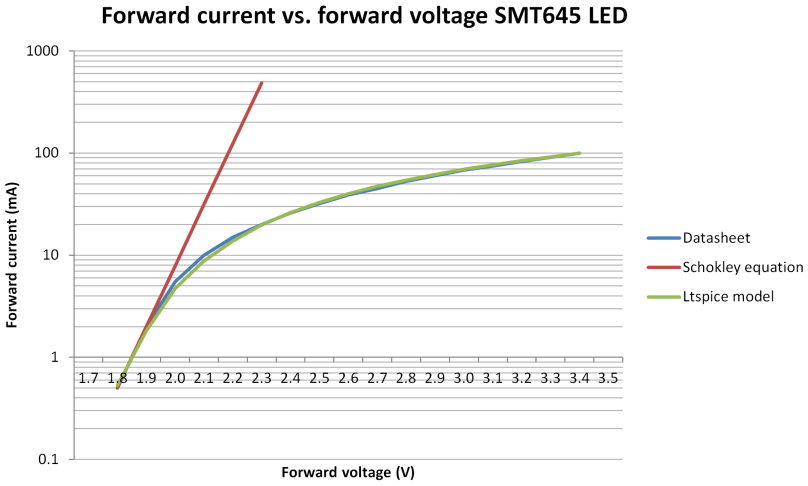

Figure A.5: Excel plot showing the forward current forward voltage relationship of the red SMT645 LED based on the datasheet, Shokley diode equation and LTspice model.

A.2.3. Junction capacitance

The junction capacitance will determine the rise and fall time of the forward current through the LED in a transient event. The junction capacitance was not stated in the datasheets and thus need to be estimated. The other LEDs in the diode library of LTspice have a capacitance of 50pF. This value was also taken for the LTspice models of the SMT470, SMT645 and SMT940D LEDs.

A.2.4. Saturation current temperature exponential

The IV relationship of the LEDs is influenced by the ambient temperature. The forward voltage decreases as the temperature increases for a given forward current. The saturation current temperature exponential determines how much the forward voltage is influenced by changing ambient temperature.

The LTspice library entry for the LED model needs to be changed to **.model ledtest D (Is='value for Is' N='value for N' Rs=10 Cjo=50p Xti=100)**. The value for Xti is set at 100 for now, this value will need to be changed to fit

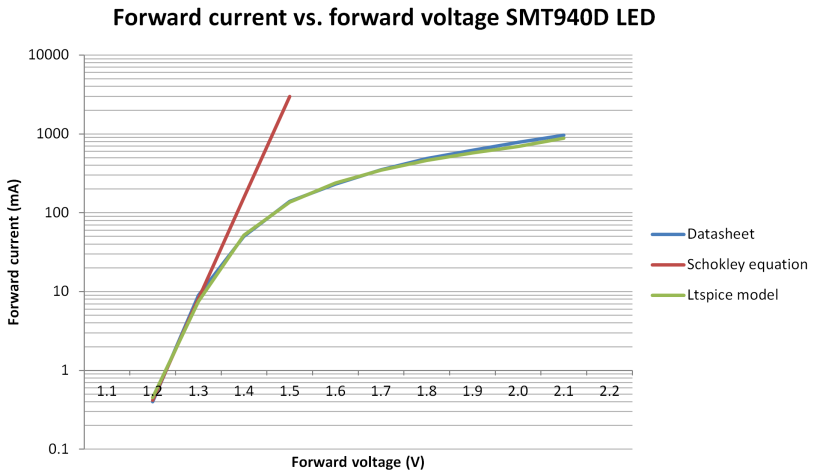

Figure A.6: Excel plot showing the forward current forward voltage relationship of the IR SMT940D LED based on the datasheet, Shokley diode equation and LTspice model.

the datasheet.

To determine the final value for Xti the LTspice model for the LED needs to be connected to a constant current source set at 20mA for the blue and red LED and 50mA for the IR LED, this are the currents used to illustrate the influence of temperature on the forward voltage in the datasheets. A simulation using a temperature sweep is performed and the voltage across the LED is measured. The Xti value needs to be given such a value that the LTspice plot matches that found in the datasheet.

After the value for Xti is found all five parameters for the LTspice models have been acquired. These LED models can be used for future LTspice simulations for designing a LED driver.

A.3. In depth design and simulation of MOSFET based LED Driver

The following part of the appendix describes in greater detail the MOSFET based LED driver design featured in section 5.2.4. It will furthermore give proof of proper operation using LTspice simulations.

The MOSFET based LED driver circuit is conceptually simple and uses just two resistors and a MOSFET to drive the LED. Figure A.7 shows the circuit. The LTspice model for the SMT470 made as described at the end of section 5.2.3 and appendix A.2 was used. The LTspice model for the RUM001L02 MOSFET was obtained from the manufacturer Rohm Semiconductors [32] and is used to make a customized component in LTspice using the code shown in A.4.

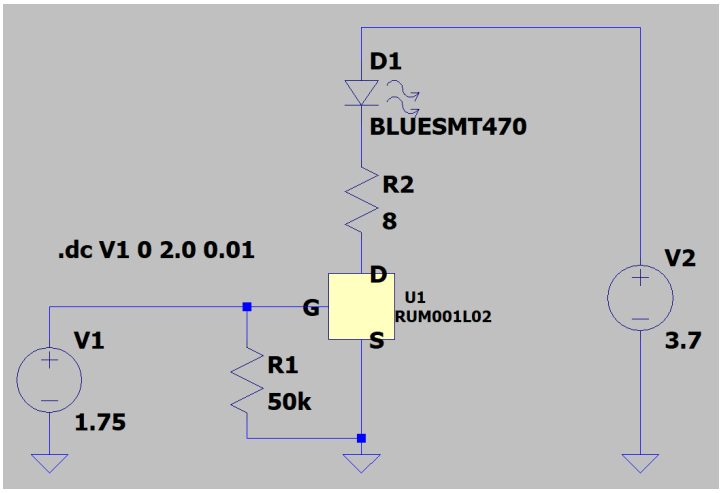

Figure A.7: LED driver schematic for blue SMT470 LED. Forward current LED is 45 mA at 1.75V MOSFET gate-source voltage.

Listing A.4: LTspice model for RUM001L02 obtained from the manufacturer Rohm Semiconductors

```
**********D G S
.SUBCKT RUM001L02 1 2 3
M1 11 22 3 3 MOS_N
D1 3 1 DDS
R1 1 11 RTH 2.01
D2 22 11 DDG
R2 2 22 326
.MODEL MOS_N NMOS
+ LEVEL=3
+ L=2.0000E-6
+ W=0.1
+ KP=1.0399E-5
+ RS=10.000E-3
+ RD=0
+ VTO=.69971
+ RDS=20.000E6
+ TOX=2.0000E-6
+ CGSO=41p
+ CGDO=10p
+ CBD=0
+ RG=0
+ N=2
+ RB=1.0000E-3
+ GAMMA=0.3
+ ETA=0.0001
+ KAPPA=0
+ NFS=8G
.MODEL DDS D
+ IS=1.2632E-12
+ N=1.2237
+ RS=.1162
+ IKF=53.751E-3
+ CJO=3.9172E-12
+ M=.338
+ VJ=.76101
+ BV=20
+ TT=21n
.MODEL DDG D
+ CJO=4.0345E-12
+ M=.66305
```

```
+ VJ=.76707
+ N=10000
+ FC=0.5
.MODEL RTH RES
+ TC1=0.0055
+ TC2=0.000005
.ENDS RUM001L02
```

MOSFETs have a small gate capacitance that is charged when voltage is applied to the gate. When the voltage supply tot the gate is removed the gate capacitance remains high for a brief period. To overcome this a large resistance is connected between gate and ground to discharge the capacitor. It furthermore ensures the gate is never floating, which could cause unwanted behaviour. The value is not very import, somewhere between 10kΩ and 100kΩ. A value of 50kΩ was chosen.

Resistor R2 is placed in series with the LED to limit the current through the LED when the MOSFET is operating in the saturation region. For the blue SMT470 LED requiring 45 mA of forward current a resistance of 8Ω is needed. This is proven by the simulations, see figure A.8. For the red SMT645 LED also requiring 45 mA of forward current 19Ω of resistance is added in series. Finally for the IR SMT940D LED 21Ω is used to obtain a forward current of 26 mA. These values were also obtained using simulations.

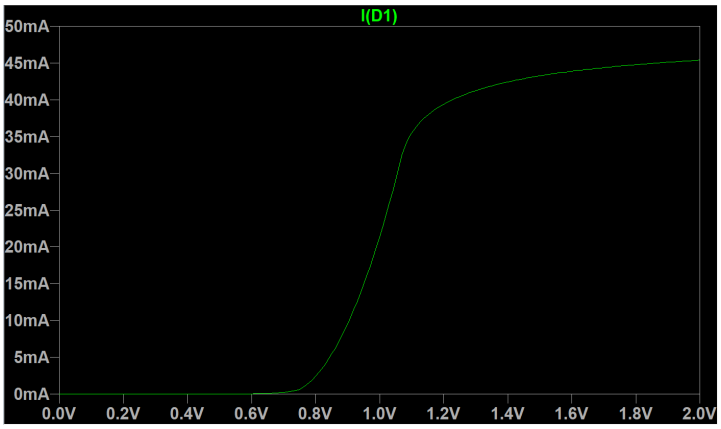

Figure A.8: LTspice DC sweep simulation illustrating the effect of an increasing MOSFET gate-source voltage on the forward current through the LED.

The simulation shown in figure A.8 also proves the MOSFETs changes between operation modes at the proper gate voltages. At a gate voltage between 0 and 0.25V, the low state output voltage of the MCU GPIO pin, the MOSFET prevents current from flowing through the LED. With a gate voltage ranging from 1.75 to 2V, the high state output voltage, The MOSFET is in active saturation mode and passes the desired current. The same type of simualtion was performed for the other two LEDs and gave the same desired MOSFET states for the potential gate voltages.

In section 5.2.4 figure 5.3 shows the schematic containing the three LEDs and their drivers. The circuit is simulated in time using three pulsating voltage sources with a period of 100us and an on time of 20us. The three sources are delayed with $\frac{100}{3}$us in relationship to one an other. This ensures no more than one LED is on at a given time. Similar control signals will be used when the PPG sensor is in operation. The result of the simulation is given in figure A.9.

The simulation shows the desired forward currents through the LEDs at the wanted times. There is however a small delay when the LEDs switch states most probably caused by capacitance's within the components. As there is a clear separation between when two individual LEDs are in the on-state there is no reason for concern.

The influence of ambient temperature on the LEDs and drivers is also an important factor to explore and take in to account. Figure A.10 is the same simulation as shown in figure A.9, however now it has been performed

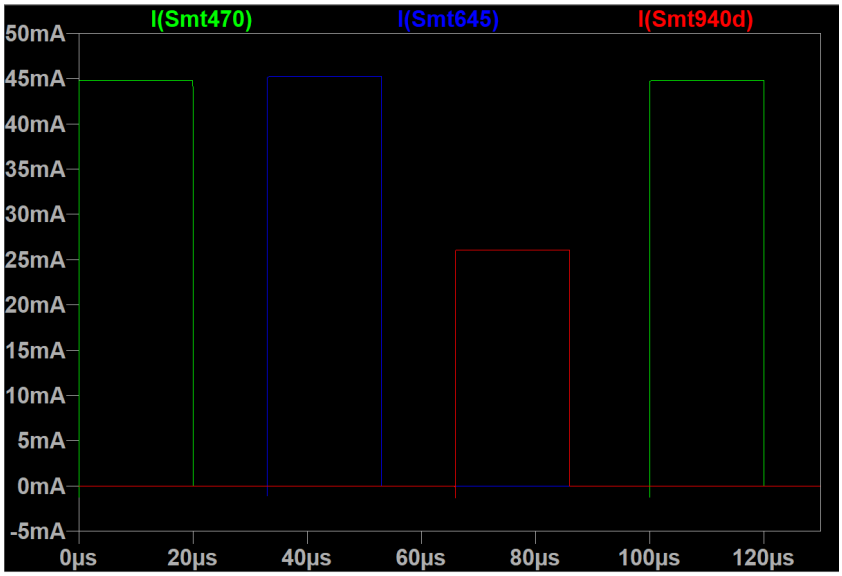

Figure A.9: LTspice simulation of the three LEDs and their drivers using a pulsing voltage sources connected to the gates of the MOSFETs.

under 20, 30 and 40 °C. At higher temperatures more forward current is experienced by the LEDs than at lower temperatures. The influence of temperature is most dominant in the blue and red LED as these have a higher saturation current temperature exponential (Xti) compared to the IR LED, experiencing hardly any influence of temperature. Between 20 and 40 °C, there is a difference of less than 2 mA of forward current for the blue and red LEDs. The influence of temperature on the light output of the LED is not large enough to be of concern.

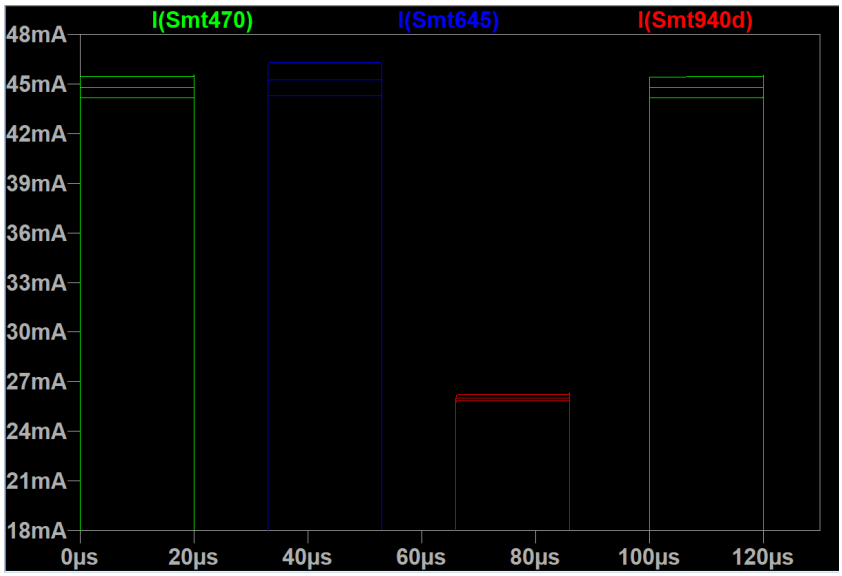

Figure A.10: LTspice simulation at 20, 30 and 40 °C of the three LEDs and their drivers using a pulsing voltage sources connected to the gates of the MOSFETs.

A final power simulation is required to obtain a better understanding of the energy consumption and efficiency. The simulation performed in A.9 was used to obtain the power consumption of all components, see table A.1.

Table A.1: Power consumption of LEDs and LED driver components

Component	Power consumption (mW)	Fraction of delivered power
3.7V power supply (blue LED ON)	**-166 (Delivered)**	**1**
blue SMT470 LED	142	0.855
8Ω resistor	16	0.096
MOSFET	8	0.048
3.7V power supply (red LED ON)	**-167 (Delivered)**	**1**
blue SMT470 LED	120	0.719
19Ω resistor	39	0.234
MOSFET	8	0.048
2.0V power supply (IR LED ON)	**-52 (Delivered)**	**1**
blue SMT470 LED	35	0.673
21Ω resistor	14	0.269
MOSFET	3	0.058

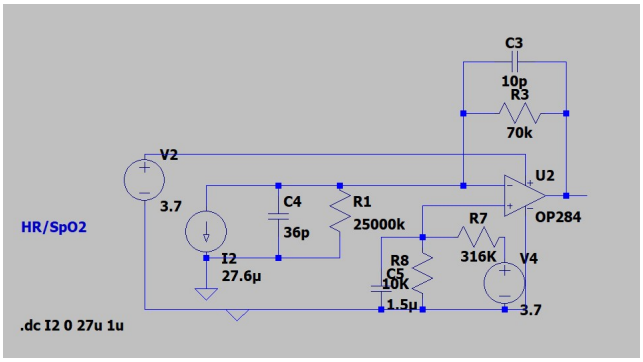

Figure A.11: Bilirubin sensor model

A.4. Photodiode and transimpedance amplifier

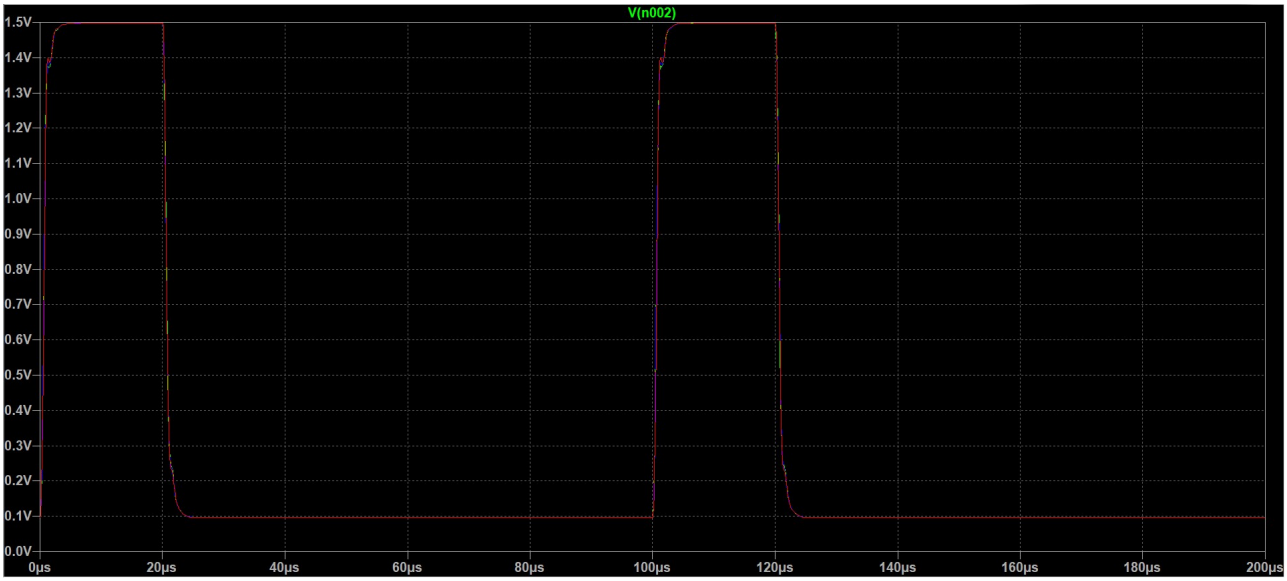

Figure A.12: Heart rate and oxygen saturation sensor temperature dependence

B

List of Components

Table B.1: The list of components needed to construct all sensors

Component	Amount	Size (L x W x H in mm)	Price p.p.
Temperature Sensor			
Si7051 SMD	1	3 x 3 x 0.75	1,76
10kΩ resistor SMD 0.1% APC0201	2	0.58 x 0.29 x 0.23	0,39
0.1 uF capacitor SMD 10% KEMET 0603	1	1.6 x 0.8 x 0.8	0,24
Acceleration Sensor			
IIS2DLPC SMD	1	2 x 2 x 0.7	2,03
0.1 uF capacitor SMD 10% KEMET 0603	1	1.6 x 0.8 x 0.8	0,24
10 uF capacitor SMD 10% Taiyo Yuden 0603	1	1.6 x 0.8 x 0.45	0,27
10kΩ resistor SMD 0.1% APC0201	2	0.58 x 0.29 x 0.23	0,39
PPG Sensor - LEDs			
Ushio SMT470 blue LED	1	3.5 x 2.7 x 1.8	0,73
Ushio SMT645 red LED	1	3.5 x 2.7 x 1.8	0,73
Ushio SMT940D infra-red LED	1	3.5 x 2.7 x 1.8	0,73
PPG Sensor - LED Drivers			
ROHM RUM001L02 MOSFET	3	1.2 x 1.2 x 0.5	0,30
50kΩ resistor SMD 0.1% Yageo	3	1.6 x 0.8 x 0.45	0,34
8.2 Ω resistor SMD 0.1% Yageo	1	1.6 x 0.8 x 0.45	0,31
19.1 Ω resistor SMD 0.1% TE Connectivity	1	1.0 x 0.5 x 0.3	0,38
21 Ω resistor SMD 0.1% TE Connectivity	1	1.0 x 0.5 x 0.3	0,41
PPG Sensor - Photodiodes			
VEMD5510C blue photodiode	1	5 x 4 x 0.9	1,84
PDB-C160SM red/ir photodiode	1	4.39 x 3.84 x 1.14	4,71
PPG Sensor - Amplifiers			
OP284 operational amplifier	1	9.27 x 6.35 x 3.3	3.82
10pF capacitor Kemet	2	1 x 0.5 x 0.5	0.11
70 $k\Omega$ resistor Vishay	1	6.1 x 2.26 x 2.26	0,19
120 $k\Omega$ resistor KOA Speer	1	2.3 x 2.3 x 6.1	
1.5 pF capacitor Murata	2	1 x 0.5 x 0.55	0,21
320 $k\Omega$ resistor Yageo	2	1.6 x 0.8 x 0.45	0,18
10 $k\Omega$ resistor Yageo	2	2 x 1.25 x 0.5	0,10

Bibliography

[1] URL https://www.umcutrecht.nl/en/research/researchers/dudink-jeroen-j. J. Dudink is a specialist in neonatology and neoroscience. From 2004 to 2016 he has worked as a neonatologist and researcher of neonatal neuroimaging at Erasmus Medical Center. He has further worked as a pediatrician in Leiden and neonatologist in the Sophia children's hospital of Rotterdam. J. Dudink is presently working at the Department of Neonatology at University Medical Center Utrecht.

[2] C. S. Abella, S. Bonina, A. Cucuccio, S. D'Angelo, G. Giustolisi, A. D. Grasso, A. Imbruglia, G. S. Mauro, G. A. M. Nastasi, G. Palumbo, S. Pennisi, G. Sorbello, and A. Scuderi. Autonomous energy-efficient wireless sensor network platform for home/office automation. *IEEE Sensors Journal*, 19(9):3501–3512, 2019.

[3] Kittidej Arthittayapiwat, Prapawadee Pirompol, and Pranchalee Samanpiboon. Chest expansion measurement in 3-dimension by using accelerometers. *Engineering Journal*, 23:71–84, 03 2019. doi: 10.4186/ej.2019.23.2.71.

[4] Paul Beard. Biomedical photoacoustic imaging. *Interface Focus*, 2011:602–632, 06 2011. doi: 10.1098/rsfs.2011.0028. URL http://doi.org/10.1098/rsfs.2011.0028.

[5] J. K. Brown, D. Abdallah, J. Boley, N. Collins, K. Craig, G. Glennon, K. Huang, C. J. Lukas, W. Moore, R. K. Sawyer, Y. Shakhsheer, F. B. Yahya, A. Wang, N. E. Roberts, D. D. Wentzloff, and B. H. Calhoun. 27.1 a 65nm energy-harvesting ulp soc with 256kb cortex-m0 enabling an 89.1µw continuous machine health monitoring wireless self-powered system. In *2020 IEEE International Solid- State Circuits Conference - (ISSCC)*, pages 420–422, 2020.

[6] J. Chien. A 1.8-ghz near-field dielectric plethysmography heart-rate sensor with time-based edge sampling. *IEEE Journal of Solid-State Circuits*, 55(3):615–628, 2020.

[7] T. Elfaramawy, C. Latyr Fall, M. Morissette, F. Lellouche, and B. Gosselin. Wireless respiratory monitoring and coughing detection using a wearable patch sensor network. In *2017 15th IEEE International New Circuits and Systems Conference (NEWCAS)*, pages 197–200, 2017.

[8] T. Elfaramawy, C. L. Fall, S. Arab, M. Morissette, F. Lellouche, and B. Gosselin. A wireless respiratory monitoring system using a wearable patch sensor network. *IEEE Sensors Journal*, 19(2):650–657, 2019.

[9] Renée Flacking, Liisa Lehtonen, Gill Thomson, Anna Axelin, Sari Ahlqvist, Victoria Hall Moran, Uwe Ewald, Fiona Dykes, and the SCENE group. Closeness and separation in neonatal intensive care. *Acta Paediatrica*, 101(10):1032–1037, 2012. doi: 10.1111/j.1651-2227.2012.02787.x. URL https://onlinelibrary.wiley.com/doi/abs/10.1111/j.1651-2227.2012.02787.x.

[10] Macaveiu Gabriela. Mathematical methods in biomedical optics. *ISRN Biomedical Engineering*, 2013:1–8, 01 2013. doi: 10.1155/2013/464293.

[11] Nederlands Huisarten Genootschap. Reiniging en desinfectie of sterilisatie van instrumentarium, 2018. URL https://www.nhg.org/themas/publicaties/reiniging-en-desinfectie-sterilisatie-van-instrumentarium.

[12] Qing-Song Zhu Bang-Yu Huang Guan-Zheng Liu, Yan-Wei Guo and Lei Wang. Estimation of respiration rate from three-dimensional acceleration data based on body sensor network. *Telemedicine and e-Health*, 17(9):705–711, 2011. doi: 10.1089/tmj.2011.0022.

[13] M Hickey and P A Kyriacou. Optimal spacing between transmitting and receiving optical fibres in reflectance pulse oximetry. *Journal of Physics: Conference Series*, 85:012030, oct 2007. doi: 10.1088/1742-6596/85/1/012030. URL https://doi.org/10.1088%2F1742-6596%2F85%2F1%2F012030.

[14] P. D. Hung, S. Bonnet, R. Guillemaud, E. Castelli, and P. T. N. Yen. Estimation of respiratory waveform using an accelerometer. In *2008 5th IEEE International Symposium on Biomedical Imaging: From Nano to Macro*, pages 1493–1496, 2008.

[15] E. Jovanov. Vital sign monitoring using capacitive sensing. In *2018 40th Annual International Conference of the IEEE Engineering in Medicine and Biology Society (EMBC)*, pages 5930–5933, 2018.

[16] Yunus Karamavuş and Mehmed Özkan. Newborn jaundice determination by reflectance spectroscopy using multiple polynomial regression, neural network, and support vector regression. *Biomedical Signal Processing and Control*, 51:253 – 263, 2019. ISSN 1746-8094. doi: https://doi.org/10.1016/j.bspc.2019.01.019. URL http://www.sciencedirect.com/science/article/pii/S1746809419300199.

[17] Hyung-Jik Lee and Seul Jung. Gyro sensor drift compensation by kalman filter to control a mobile inverted pendulum robot system. pages 1 – 6, 03 2009. doi: 10.1109/ICIT.2009.4939502.

[18] Mathieu Lemay, Mattia Bertschi, Josep Sola, Philippe Renevey, Jakub Parak, and Ilkka Korhonen. Chapter 2.3 - application of optical heart rate monitoring. In Edward Sazonov and Michael R. Neuman, editors, *Wearable Sensors*, pages 105 – 129. Academic Press, Oxford, 2014. ISBN 978-0-12-418662-0. doi: https://doi.org/10.1016/B978-0-12-418662-0.00023-4. URL http://www.sciencedirect.com/science/article/pii/B9780124186620000234.

[19] D. Marzorati, D. Bovio, C. Salito, L. Mainardi, and P. Cerveri. Chest wearable apparatus for cuffless continuous blood pressure measurements based on ppg and pcg signals. *IEEE Access*, 8:55424–55437, 2020.

[20] A. M. Nia, M. Mozaffari-Kermani, S. Sur-Kolay, A. Raghunathan, and N. K. Jha. Energy-efficient long-term continuous personal health monitoring. *IEEE Transactions on Multi-Scale Computing Systems*, 1 (2):85–98, 2015.

[21] World Health Organization. Health-care waste, 2018. URL https://www.who.int/news-room/fact-sheets/detail/health-care-waste.

[22] *Chemical Resistance Guide for Silicone Hose*. Parker, -. URL https://www.parker.com/Literature/Fluid%20Transfer%20Hose%20-%20Europe/chemical%20table%20silicone.pdf.

[23] Merja Puurtinen, Jari Viik, and Jari Hyttinen. Best electrode locations for a small bipolar ecg device: Signal strength analysis of clinical data. *Annals of Biomedical Engineering*, 37(2):331–336, Feb 2009. ISSN 1573-9686. doi: 10.1007/s10439-008-9604-y. URL https://doi.org/10.1007/s10439-008-9604-y.

[24] T. Reinvuo, M. Hannula, H. Sorvoja, E. Alasaarela, and R. Myllyla. Measurement of respiratory rate with high-resolution accelerometer and emfit pressure sensor. In *Proceedings of the 2006 IEEE Sensors Applications Symposium, 2006.*, pages 192–195, 2006.

[25] Nicholas Rutter and Len Doyal. Neonatal care and management of pain: Historical and ethical issues. *Seminars in Neonatology*, 3(4):297 – 302, 1998. ISSN 1084-2756. doi: https://doi.org/10.1016/S1084-2756(98)80084-5. URL http://www.sciencedirect.com/science/article/pii/S1084275698800845.

[26] Laxminarayan S, Rakesh V, Oyama T, and et al. Individualized estimation of human core body temperature using noninvasive measurements. *J Appl Physiol (1985)*, 124(6):1387–1402, 2018. doi: 10.1152/japplphysiol.00837.2017.

[27] A. Sabban. Small new wearable antennas for iot, medical and sport applications. In *2019 13th European Conference on Antennas and Propagation (EuCAP)*, pages 1–5, 2019.

[28] J. M. Schmitt, G. X. Zhou, E. C. Walker, and R. T. Wall. Multilayer model of photon diffusion in skin. *J. Opt. Soc. Am. A*, 7(11):2141–2153, Nov 1990. doi: 10.1364/JOSAA.7.002141. URL http://josaa.osa.org/abstract.cfm?URI=josaa-7-11-2141.

[29] JM Schmitt, GX Zhou, EC Walker, and RT Wall. Multilayer model of photon diffusion in skin. *Journal of the Optical Society of America. A, Optics and image science*, 7(11):2141—2153, November 1990. ISSN 0740-3232. doi: 10.1364/josaa.7.002141. URL https://doi.org/10.1364/josaa.7.002141.

[30] Alina Sekretaryova. Chapter 4 - powering wearable bioelectronic devices. In Onur Parlak, Alberto Salleo, and Anthony Turner, editors, *Wearable Bioelectronics*, Materials Today, pages 89 – 132. Elsevier, 2020. ISBN 978-0-08-102407-2. doi: https://doi.org/10.1016/B978-0-08-102407-2.00005-9. URL http://www.sciencedirect.com/science/article/pii/B9780081024072000059.

[31] OSRAM Opto Semiconductors. Biofy®, sfh 7050, biomonitoring sensor, . URL https://www.osram.com/ecat/BIOFY%C2%AE%20SFH%207050/com/en/class_pim_web_catalog_103489/global/prd_pim_device_2220012/. Accessed on: June 18, 2020.

[32] ROHM Semiconductors. Small signal mosfets, . URL https://www.rohm.com/products/mosfets/small-signal. Accessed on: June 18, 2020.

[33] N. Wuthibenjaphonchai, M. Haruta, T. Noda, K. Sasagawa, T. Tokuda, M. Sawan, S. Carrara, and J. Ohta. Battery-free. sticker-like, device for health monitoring, operated by optical power transfer. In *2018 IEEE Biomedical Circuits and Systems Conference (BioCAS)*, pages 1–4, 2018.

[34] Dmitriy Zhdanov, A. Bureev, Liudmila Khokhlova, A.I. Seleznev, and Ivan Zemlyakov. Short review of devices for detection of human breath sounds and heart tones. *Biology and Medicine*, 6, 01 2014.